

## Supporting Information for

### Long-Range Electrostatic Effects from Intramolecular Lewis Acid Binding Influence the Redox Properties of Cobalt-Porphyrin Complexes

Jose L. Alvarez-Hernandez,<sup>a,†</sup> Xiaowei Zhang,<sup>b,†</sup> Kai Cui,<sup>c</sup> Anthony P. Deziel,<sup>a</sup> Sharon Hammes-Schiffer,<sup>c,\*</sup> Nilay Hazari,<sup>a,\*</sup> Nicole Piekut,<sup>a</sup> & Mingjiang Zhong<sup>b,\*</sup>

<sup>†</sup>Authors contributed equally.

<sup>a</sup>Department of Chemistry, Yale University, New Haven CT 06520, United States. E-mail: [nilay.hazari@yale.edu](mailto:nilay.hazari@yale.edu)

<sup>b</sup>Department of Chemical and Environmental Engineering, Yale University, New Haven CT 06520, United States. E-mail: [mingjiang.zhong@yale.edu](mailto:mingjiang.zhong@yale.edu)

<sup>c</sup>Department of Chemistry, Princeton University, Princeton, NJ 08540, United States. E-mail: [shs566@princeton.edu](mailto:shs566@princeton.edu)

#### Table of Contents

<b>I. Experimental and Computational Methods .....</b>	<b>3</b>
<b>II. Synthesis and Characterization of Porphyrin Ligands.....</b>	<b>7</b>
<b>III. Synthesis and Characterization of Cobalt-Porphyrin Complexes.....</b>	<b>10</b>
<b>IV. Lewis Acid Binding to 1: HRMS.....</b>	<b>17</b>
<b>V. Lewis Acid Binding to 1: Variable Temperature <sup>7</sup>Li and <sup>19</sup>F NMR Spectroscopy .....</b>	<b>20</b>
<b>VI. Li<sup>+</sup> Binding to 1: <sup>7</sup>Li and <sup>1</sup>H NMR Spectroscopy, Job Plot .....</b>	<b>26</b>
<b>VII. Determination of Binding Constants: Nonlinear Fitting.....</b>	<b>28</b>
<b>VIII. Li<sup>+</sup> Binding to Free Crown: <sup>7</sup>Li and <sup>1</sup>H NMR Spectroscopy, Job Plot.....</b>	<b>29</b>
<b>VIII. Other Lewis Acids Binding to 1: Titrations monitored by <sup>1</sup>H NMR Spectroscopy ..</b>	<b>31</b>
<b>IX. Cyclic Voltammograms in the Presence of TBAOTf .....</b>	<b>34</b>
<b>X. Cyclic Voltammograms in the Presence of Lewis Acids.....</b>	<b>35</b>
<b>XI. Impact of Ca(OTf)<sub>2</sub> on the Ligand-Centered Redox Couple .....</b>	<b>41</b>
<b>XI. Cyclic Voltammograms with Trivalent Cations .....</b>	<b>42</b>
<b>XII. Cyclic Voltammograms at Varying Ionic Strengths.....</b>	<b>43</b>

<b>XIII. Computational Results.....</b>	<b>45</b>
<b>XIV. Including Ionic Strength and Counterion Effects in the Computational Model .....</b>	<b>47</b>
<b>XV. Electrocatalytic CO<sub>2</sub> Reduction and Catalyst Deactivation.....</b>	<b>62</b>
<b>XVI. References.....</b>	<b>64</b>

## I. Experimental and Computational Methods

### *Materials*

Chemicals used in the preparation of complexes **1** and **2** were used as received from Sigma Aldrich, Acros Organics, Alfa Aesar, or TCI unless otherwise specified. ACS grade solvents were used as received from Sigma Aldrich and Macron Fine Chemicals. Silica gel was purchased from Sorbtech (standard grade) with 60 Å porosity and 40 – 63 µm particle size. Analytical thin layer chromatography (TLC) was performed on Merck precoated TLC plates (silica gel 60 GF254, 0.25 mm).

Triflate salts were purchased from Sigma Aldrich (at least 98% purity). Lithium, sodium, calcium, barium, and tetrabutylammonium triflates were used as purchased. Potassium and strontium triflates were dissolved in acetonitrile yielding a very fine suspension that was filtered through a silica plug and the solvent removed under vacuum. Acetonitrile used for electrochemistry experiments was obtained from a solvent Inert Technologies PureSolv MD7 solvent purification system and subsequently stored under N<sub>2</sub>. The water content was determined to be ~30 ppm using a Karl-Fischer Titrator. Tetrabutylammonium hexafluorophosphate (TBAPF<sub>6</sub>) was purchased from Sigma Aldrich and recrystallized three times from ethanol. The solid was dried under vacuum for three days. Ferrocene was purchased from Sigma Aldrich and used as received. All electrodes were purchased from CH Instruments Inc. Deuterated solvents were purchased from Cambridge Isotope Laboratories Inc. and stored over activated molecular sieves.

### *Spectroscopic/Spectrometric Methods*

UV-vis Spectroscopy. UV-vis spectra were collected in dichloromethane, using a quartz cuvette with a 1 cm path length in a Shimadzu UV-3600 Plus Spectrophotometer.

NMR Spectroscopy. <sup>1</sup>H and <sup>13</sup>C{<sup>1</sup>H} NMR spectra for the characterization of ligands and complexes were recorded on an Agilent DD2 400 MHz spectrometer (101 MHz <sup>13</sup>C frequency). <sup>1</sup>H, <sup>7</sup>Li, and <sup>19</sup>F NMR spectra for the Lewis acid binding studies were run in an Agilent DD2 500 MHz spectrometer (194 MHz <sup>7</sup>Li and 470 MHz <sup>19</sup>F frequencies). In all cases relaxation times were set to 1 s and spectra referenced versus the solvent residual signals. For <sup>7</sup>Li and <sup>19</sup>F NMR spectra, a <sup>1</sup>H spectrum was collected and used as absolute reference.

EPR Spectroscopy. Electron paramagnetic resonance spectra were collected on a Bruker EleXsys EPR Spectrometer in X-band mode at 7 K in toluene. Spectra were simulated using the pepper core function in the EasySpin 5.2.35 program, operated in MATLAB.<sup>1</sup>

HRMS. High resolution mass spectrometry was conducted in a Shimadzu 9030 Quadrupole mass spectrometer with electrospray ionization.

### *Fitting of <sup>7</sup>Li NMR Spectroscopic Data to Determine Binding Constants*

Binding constants ( $K_b$ ) were determined by fitting the <sup>7</sup>Li NMR spectra collected at increasing LiOTf molar equivalents relative to **1** or free aza-crown (structure shown in Figure S30) to equation 2 of the main text. This non-linear least square fitting was performed iteratively using the curve\_fit function in the Scipy module.<sup>2</sup> The parameters fitted were  $K_b$ ,  $\delta_{Li}$ , and  $\delta_{ML}$ ; the initial

values used in the iterative fitting were  $4 \times 10^4$ , -2.6 and -0.6 respectively. The outputs of the fittings are shown in Figures S27 and S28.

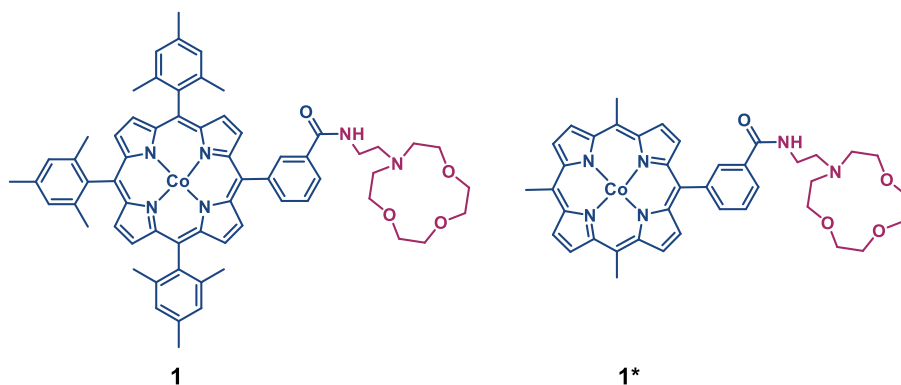
### *Electrochemical Studies*

Cyclic Voltammetry. Cyclic Voltammetry experiments were conducted in acetonitrile using TBAPF<sub>6</sub> as supporting electrolyte. A three-electrode system was utilized comprising of glassy carbon (GCE) as the working electrode (3 mm diameter) with a geometric surface area (A) of  $\sim 7.07 \times 10^{-2}$  cm<sup>2</sup>, a Pt wire counter electrode (A  $\sim 0.49$  cm<sup>2</sup>), and a silver wire pseudo-reference electrode with 1 mM ferrocene as internal standard. A CHI 720E potentiostat was used for all electrochemical measurements. Cyclic voltammograms were collected scanning cathodically from the more positive to the more negative potentials and then in the anodic direction within the same potential window. All cyclic voltammograms were performed with 1 mM ferrocene and then in the absence of it to evaluate the Co(III)/Co(II) couple which overlaps with the Fc<sup>+</sup>/Fc couple. Cyclic voltammograms collected without ferrocene were referenced vs. Fc<sup>+</sup>/Fc based on the Co(II)/Co(I) couple, which was unaltered by the addition of ferrocene. The GCE was polished using 0.05  $\mu$ m on a felt pad, thoroughly rinsed, and sonicated prior to the collection of cyclic voltammograms. The working solution for cyclic voltammetry was purged with Ar or CO<sub>2</sub>, as indicated, for 10 minutes, then the headspace was kept under a constant flow of the specified gas for the duration of the experiment.

Bulk Electrolysis and Product Analysis. Controlled potential electrolysis (CPE) was conducted in a gas-tight two-compartment cell using a three-electrode setup. The working and counter electrodes were glassy carbon rods with geometric surface areas of  $\sim 1.0$  and  $2.0$  cm<sup>2</sup> respectively, a silver wire pseudo-reference was used in the working compartment with 1 mM ferrocene as an internal standard. The two compartments were separated by a glass frit of average pore size of  $1.0$   $\mu$ m. The solutions used in CPE were purged with CO<sub>2</sub> for 15 minutes and then kept sealed for the duration of the experiment. The CPE purging gas contains 5% vol. of CH<sub>4</sub> as internal standard for product quantification. The amount of generated H<sub>2</sub> and CO was determined by gas chromatography (GC) using calibration curves obtained by injecting known volumes of H<sub>2</sub> and CO at 1 atm. The GC instrument was a Shimadzu Nexis 8030 with two capillary columns and dual thermal conductivity (TCD) and flame ionization (FID) detectors. The GC system includes a methanizer preceding FID detection to increase sensitivity to CO and CO<sub>2</sub>. Column specifications: 1 Shimadzu Q-Bond 30 m long, 0.53 mm ID, 20  $\mu$ m film thickness; and 2 Shimadzu Msieve 5A 30 m long, 0.53 mm ID, 50  $\mu$ m film thickness.

### *Computational Studies*

Conformational sampling. To reduce the computational cost, the mesityl groups on the porphyrin of **1** were replaced by methyl groups. The resulting compound is denoted **1\*** and is shown below. The conformational sampling was performed for **1\***-Ca<sup>2+</sup> with a Co(I) center (no axial acetonitrile ligand) using the Conformer-Rotamer Ensemble Sampling Tool (CREST).<sup>3</sup> In this procedure, the geometry of **1\***-Ca<sup>2+</sup> was first optimized using a density functional tight-binding (DFTB) method, GFN2-xTB,<sup>4</sup> in implicit acetonitrile solvent. Then a metadynamics-based search algorithm was used to find conformers that are local minima at the same level of theory.<sup>5</sup> The resulting conformers were manually screened to determine the starting geometries used for the subsequent DFT calculations of **1\*** with all LAs.



**DFT calculations.** All DFT calculations were performed using the Gaussian 16 package<sup>6</sup> with the BP86 functional<sup>7</sup> and the D3 empirical dispersion correction.<sup>8</sup> The LANL2DZ basis set<sup>9</sup> was used for Co and the LAs, and the 6-31G(d,p) basis set was used for the other atoms.<sup>10</sup> Spin states of  $S = \frac{1}{2}$  and  $S = 0$  were used for Co(II) and Co(I), respectively. The implicit solvent was described using the conductor-like polarizable continuum model (C-PCM)<sup>11</sup> with the dielectric constant set to 35.688 to model acetonitrile. Non-electrostatic contributions of dispersion, repulsion, and cavitation energies were also included.

Among the sampled 159 conformers discussed above, several geometrically distinct conformers were manually selected to serve as the starting geometries for the DFT geometry optimizations and free energy calculations. For the calculations of **1\*** with Co(I) and Co(II) centers without an explicit axial ligand, 12 conformers were selected for **1\***-Li<sup>+</sup> and **1\***-Ca<sup>2+</sup>, and 4 conformers were selected for the other LAs. For the calculations of **1\*** with a Co(II) center and an explicit axial acetonitrile ligand, 12 conformers were selected for **1\***-Li<sup>+</sup> and **1\***-Ca<sup>2+</sup>, but only 11 and 9 optimizations converged for **1\***-Li<sup>+</sup> and **1\***-Ca<sup>2+</sup>, respectively. For the other LAs, we only performed geometry optimizations and free energy calculations starting from the most stable conformer found for **1\***-Li<sup>+</sup> and **1\***-Ca<sup>2+</sup>. The number of conformers used in the final calculations for each case is summarized in Table S1. The free energy of each conformer was obtained by a geometry optimization followed by harmonic vibrational analysis in implicit solvent. The free energies include zero-point energy and entropic contributions, and the temperature was set to 298 K. These free energies are plotted in Figures 10 and S48.

The Co(II/I) reduction potential for each LA was computed as the difference between the free energies of the Co(II) and Co(I) species for **1\***-LA, relative to this quantity for **1\*** with no LA bound. These reduction potentials were computed both with and without an axial acetonitrile ligand bound to Co(II). As we are reporting only relative reduction potentials, the free energy of the unbound acetonitrile ligand that dissociates upon reduction of Co(II) to Co(I) cancels and therefore does not need to be calculated.

**Table S1.** Number of Conformers used in the Free Energy Calculations

LA	Co(I)	Co(II) w/o axial ligand	Co(II) w/ axial ligand
Li <sup>+</sup>	12	12	11
Na <sup>+</sup>	4	4	1
K <sup>+</sup>	4	4	1
Ca <sup>2+</sup>	12	12	9
Sr <sup>2+</sup>	4	4	1
Ba <sup>2+</sup>	4	4	1

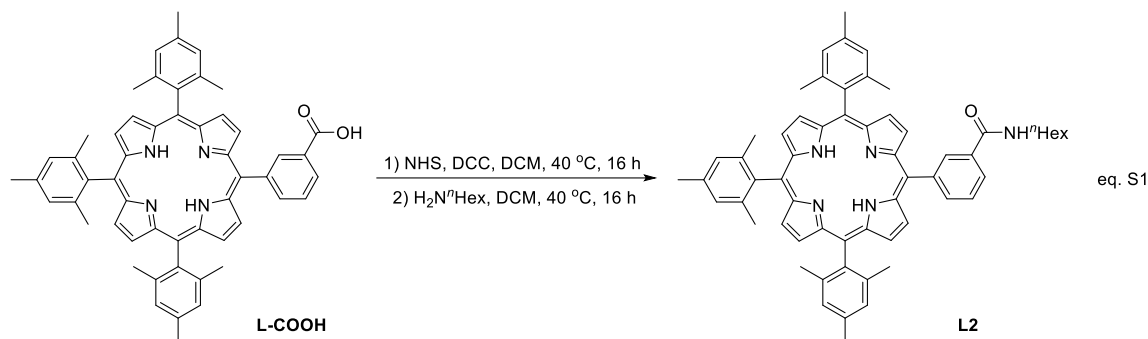
Electrostatic potential calculations. We define the electrostatic potential generated by the LA as the difference between the total electrostatic potentials of **1**\*-LA and **1**\* at the DFT-optimized geometry of **1**\*-LA. For each **1**\*-LA adduct, the electrostatic potential was calculated using the charge density corresponding to the DFT-optimized geometry of the most stable conformer. The electrostatic potential for **1**\* was computed at the same geometry as **1**\*-LA by simply removing the LA from the structure without further optimization. In this way, we eliminated the influence of geometry change on the calculated electrostatic potential. This procedure was used for each LA using the corresponding DFT-optimized geometry of **1**\*-LA, which accounts for differences in the geometries of the various adducts. The reported electrostatic potential generated by each LA at the Co center was calculated as the average within a sphere of 1 Å radius around the Co ion. The electrostatic potential was calculated on a grid with a grid spacing of 0.2 Bohr, and the averaging was performed over the grid points within the sphere.

## II. Synthesis and Characterization of Porphyrin Ligands

The ligand (**L1**) used to prepare complex **1** was synthesized as reported previously.<sup>12</sup>

### Synthesis of **L2**

The ligand **L2** used to prepare complex **2** was synthesized according to equation S1.



**L-COOH** (200 mg, 0.26 mmol) (prepared following a published procedure<sup>12</sup>) was dissolved in 10 mL anhydrous dichloromethane (DCM). Then 68 mg of N-Hydroxysuccinimide (NHS, 0.61 mmol, 2.4 equiv.) and 60 mg of N,N'-Dicyclohexylcarbodiimide (DCC, 0.61 mmol, 2.4 equiv.) were added. The solution was heated to 40 °C and stirred for 16 h, followed by addition of 200 mg of n-hexylamine ( $\text{H}_2\text{N}^n\text{Hex}$ , 2.0 mmol, 8 equiv.). The reaction mixture was left to stir for a further 16 h at 40 °C. The solution was washed with saturated aqueous  $\text{Na}_2\text{CO}_3$  solution (50 mL) and  $\text{H}_2\text{O}$  (50 mL  $\times$  3) and dried over anhydrous  $\text{Na}_2\text{SO}_4$ . The solvent was removed in vacuo. The product was purified by column chromatography on silica gel ( $\text{CH}_2\text{Cl}_2$ ,  $R_f = 0.4$ ) to afford **L2** (181 mg, yield = 82%). **L2** was characterized by UV-vis spectroscopy, as well as  $^1\text{H}$  and  $^{13}\text{C}$  NMR spectroscopies (Figures S1-S3), and HRMS.  $^1\text{H}$ -NMR (400 MHz,  $\text{CD}_2\text{Cl}_2$ ):  $\delta$  8.80 (d,  $J = 4.7$  Hz, 1H), 8.74 (d,  $J = 4.8$  Hz, 1H), 8.70 (s, 1H), 8.63 (t,  $J = 1.8$  Hz, 1H), 8.38 (d,  $J = 7.6$  Hz, 1H), 8.20 (d,  $J = 7.9$  Hz, 1H), 7.82 (d,  $J = 7.7$  Hz, 1H), 7.33 (s, 3H), 6.54 (t,  $J = 5.6$  Hz, 1H), 3.46 (dd,  $J = 7.3, 1.5$  Hz, 1H), 2.64 (s, 5H), 2.02 – 1.80 (m, 9H), 1.59 (dd,  $J = 11.5, 4.6$  Hz, 1H), 1.38 – 1.11 (m, 4H), 0.93 – 0.61 (m, 2H), -2.51 (s, 1H).  $^{13}\text{C}\{^1\text{H}\}$ -NMR (101 MHz,  $\text{CD}_2\text{Cl}_2$ ):  $\delta$  167.1, 142.4, 139.3, 139.2, 138.2, 138.0, 137.9, 136.8, 133.6, 132.2, 127.7, 127.0, 126.4, 118.1, 118.0, 118.0, 40.2, 31.5, 29.6, 26.7, 22.5, 21.4, 21.4, 21.2, 13.8. HRMS (ESI) calculated for  $\text{C}_{60}\text{H}_{62}\text{N}_5\text{O}^+$  [ $\text{M}+\text{H}^+$ ]: 868.4949, found: 868.4937. UV-Vis: Soret band: 418 nm; Q bands: 515 nm, 548 nm, 593 nm, 646 nm.

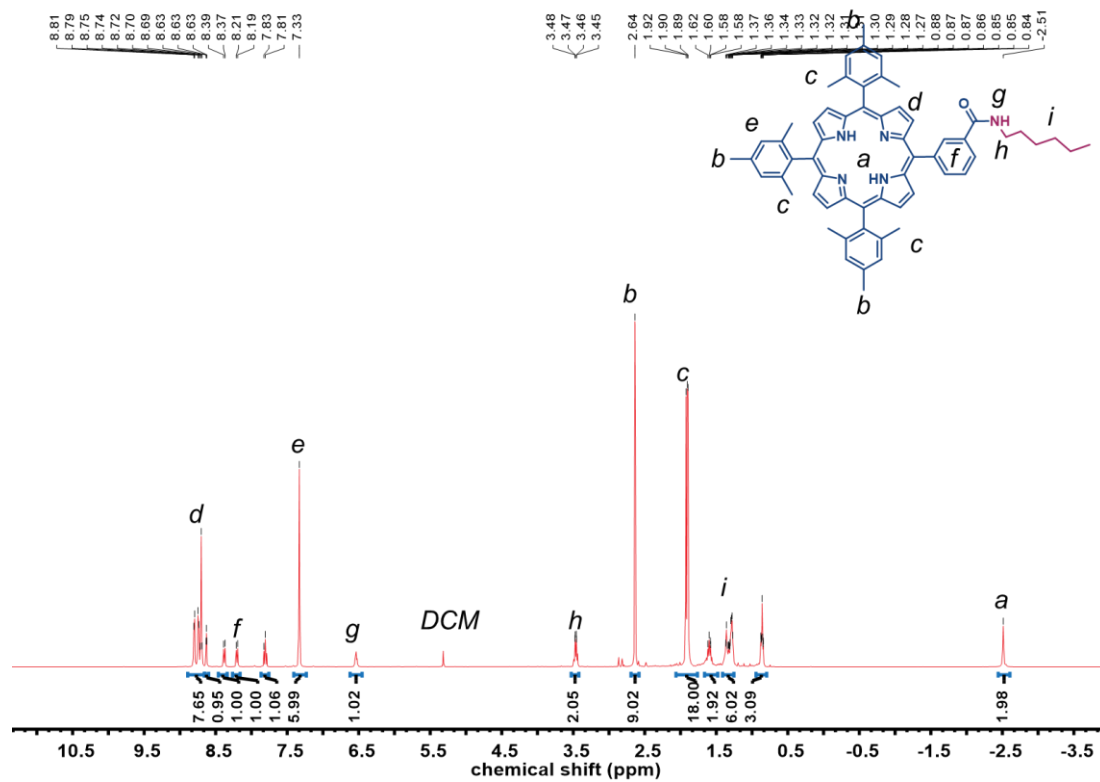


Figure S1. 400 MHz  $^1\text{H}$  NMR spectrum of **L2** in  $d_2$ -DCM.

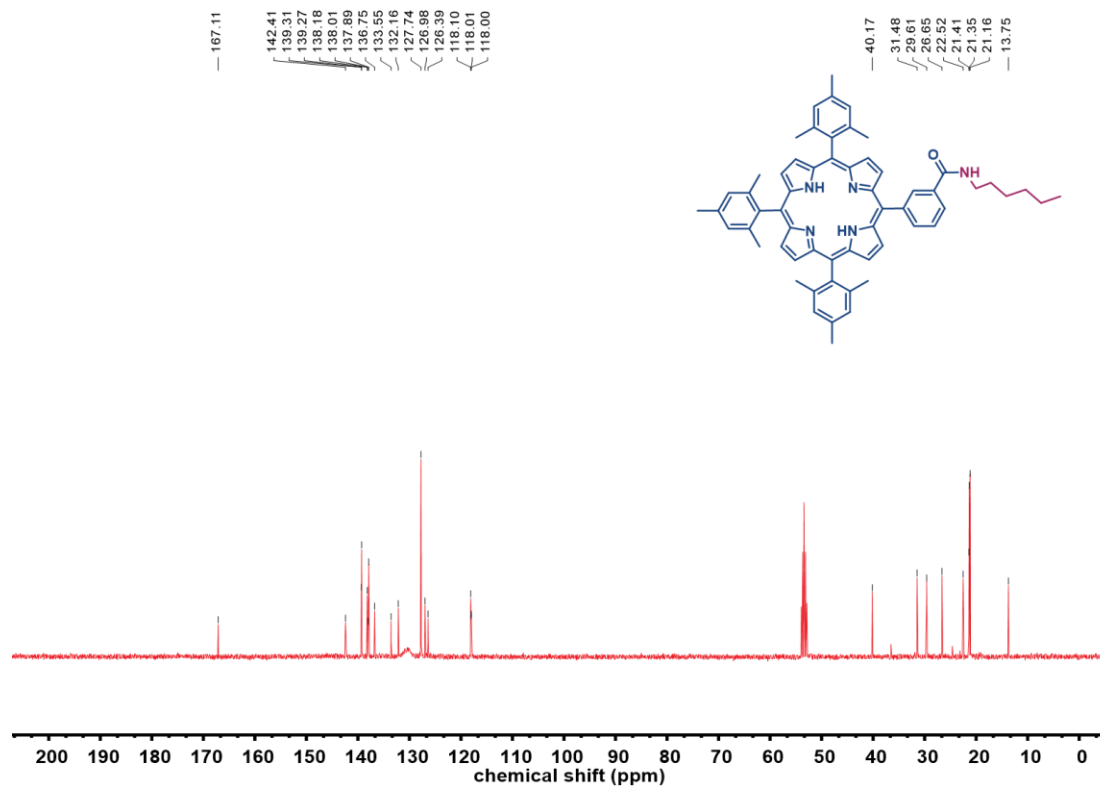
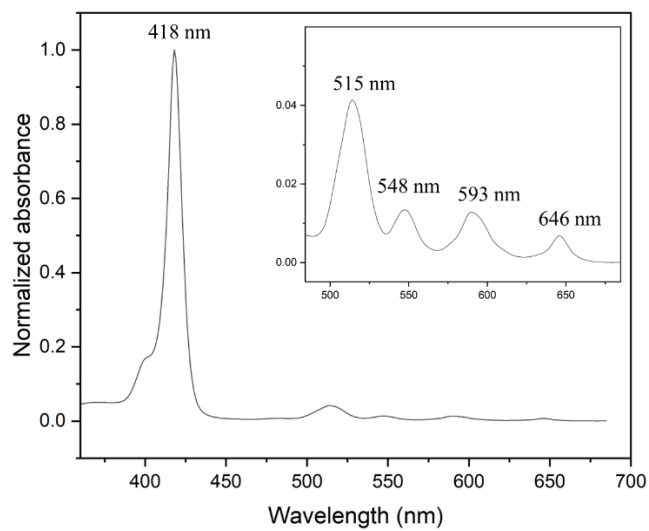


Figure S2. 101 MHz  $^{13}\text{C}\{^1\text{H}\}$  NMR spectrum of **L2** in  $d_2$ -DCM.

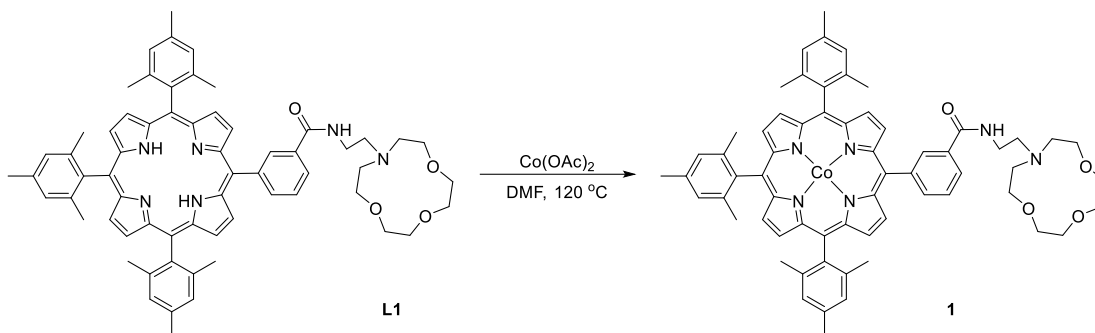


**Figure S3.** UV-vis spectrum of **L2** used in the synthesis of the control complex **2**.

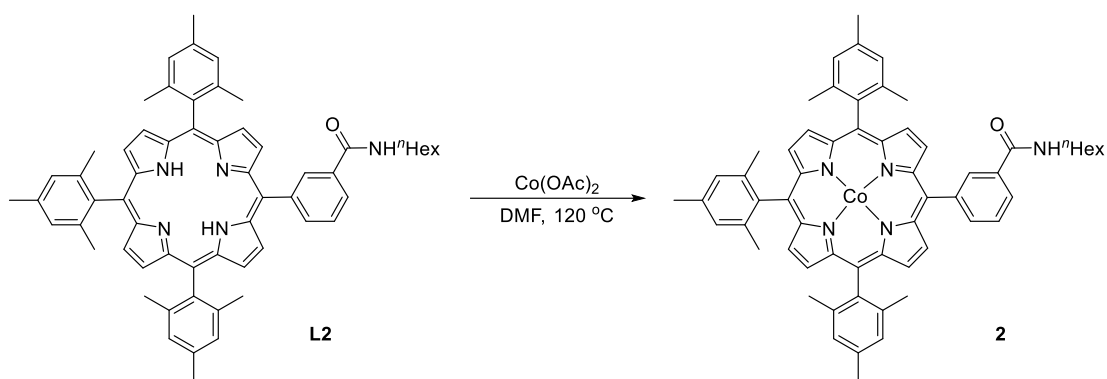
### III. Synthesis and Characterization of Cobalt-Porphyrin Complexes

Complexes **1** and **2** were prepared as described below. Characterization data is provided in Figures S4-S6 for **1**, and S7-S11 for **2**.

#### Synthesis of 1



The reaction was performed by modifying a previously published procedure.<sup>10</sup> **L1** (100 mg, 0.10 mmol) was dissolved in 20 mL of DMF, and  $\text{Co(OAc)}_2$  (85 mg, 0.51 mmol, 5 equiv.) was added. The mixture was stirred at  $120\text{ }^\circ\text{C}$  under an atmosphere of  $\text{N}_2$ . Over the course of the reaction, two additional portions of  $\text{Co(OAc)}_2$  (34 mg, 0.20 mmol, 2 equiv.) were added at intervals of 6 hours. Afterwards, the mixture was stirred for an additional 6 hours at  $120\text{ }^\circ\text{C}$ . The reaction mixture was then allowed to cool down to room temperature and the DMF was removed under reduced pressure. The residue was redissolved in 40 mL of  $\text{CH}_2\text{Cl}_2$  and washed with an aqueous solution of sodium ethylenediaminetetraacetate ( $\text{Na}_2\text{H}_2\text{EDTA}$ ) (10 mg/mL, 50 mL  $\times$  3) and  $\text{H}_2\text{O}$  (50 mL  $\times$  3). The organic layer was dried over anhydrous  $\text{Na}_2\text{SO}_4$ . The solvent was removed in vacuo, and the product was purified through column chromatography on silica gel ( $\text{CH}_2\text{Cl}_2/\text{MeOH} = 10/1$ , v/v,  $R_f = 0.3$ ) to afford **1** (90 mg, yield = 86%).  $^1\text{H-NMR}$  (400 MHz,  $\text{CD}_3\text{C}_6\text{D}_5$ ):  $\delta$  15.48 – 14.94 (8H), 12.74 (1H), 11.79 (1H), 10.28 (1H), 9.60 (8H), 7.84 (1H), 7.64 (1H), 3.99 (9H), 3.74 (12H), 3.51 (3H), 2.99 (10H), 1.76 (4H), 1.29 (4H), 0.87 (m, 4H), 0.68 (m, 4H). HRMS (ESI) calculated for  $\text{C}_{64}\text{H}_{66}\text{N}_6\text{O}_4\text{Co} [\text{M}+\text{H}^+]$ : 1042.4551, found: 1042.4651. UV-Vis: Soret band: 413 nm; Q bands: 530 nm. EPR simulation (pepper):  $g_z = 2.598$ ,  $g_y = 2.375$ ,  $g_x = 1.955$ ,  $A_z = 330\text{ MHz}$ ,  $A_y = 325\text{ MHz}$ ,  $A_x = 360\text{ MHz}$ ,  $\text{HStrain}_z = 210\text{ MHz}$ ,  $\text{HStrain}_y = 110\text{ MHz}$ ,  $\text{HStrain}_x = 80\text{ MHz}$ .



**L2** (95 mg, 0.10 mmol) was dissolved in 20 mL of DMF, and  $\text{Co(OAc)}_2$  (85 mg, 0.50 mmol, 5 equiv.) was added. The mixture was stirred at 120 °C under  $\text{N}_2$  atmosphere. Over the course of the reaction, two additional portions of  $\text{Co(OAc)}$  (34 mg, 0.20 mmol, 2 equiv.) were added at intervals of 6 hours. Afterwards, the mixture was stirred for an additional 6 hours at 120 °C. The reaction mixture was allowed to cool down to room temperature and the DMF was removed under reduced pressure. The residue was redissolved in 40 mL of  $\text{CH}_2\text{Cl}_2$  and washed with an aqueous solution of sodium ethylenediaminetetraacetate ( $\text{Na}_2\text{H}_2\text{EDTA}$ ) (10 mg/mL, 50 mL  $\times$  3), and  $\text{H}_2\text{O}$  (50 mL  $\times$  3). The organic layer was dried over anhydrous  $\text{Na}_2\text{SO}_4$ . The solvent was removed in vacuo, and the product was purified through column chromatography on silica gel ( $\text{CH}_2\text{Cl}_2$ ,  $R_f = 0.5$ ) to afford **2** (90 mg, yield = 87%).  $^1\text{H-NMR}$  (400 MHz,  $\text{CD}_3\text{C}_6\text{D}_5$ ):  $\delta$  16.42 – 16.18 (14H), 13.63 (1H), 13.19 (1H), 10.18 (1H), 9.72 (2H), 9.52 – 9.39 (12H), 3.67 (26H), 2.44 (3H), 2.25 (5H), 1.84 (5H), 1.51 (6H), 1.22 (7H), 1.05 (12H), 0.68 (7H), 0.42 (8H), 0.27 (6H) **HRMS (ESI)** calculated for  $\text{C}_{60}\text{H}_{59}\text{N}_5\text{OCo}$  [ $\text{M}^+$ ]: 924.4047, found: 924.4039. **UV-Vis**: Soret band: 413 nm; Q bands: 530 nm. **EPR simulation** (pepper):  $g_z = 3.000$ ,  $g_y = 2.700$ ,  $g_x = 1.870$ ,  $A_z = 850$  MHz,  $A_y = 830$  MHz,  $A_x = 440$  MHz,  $\text{Hstrain}_z = 300$  MHz,  $\text{Hstrain}_y = 250$  MHz,  $\text{Hstrain}_x = 100$  MHz.

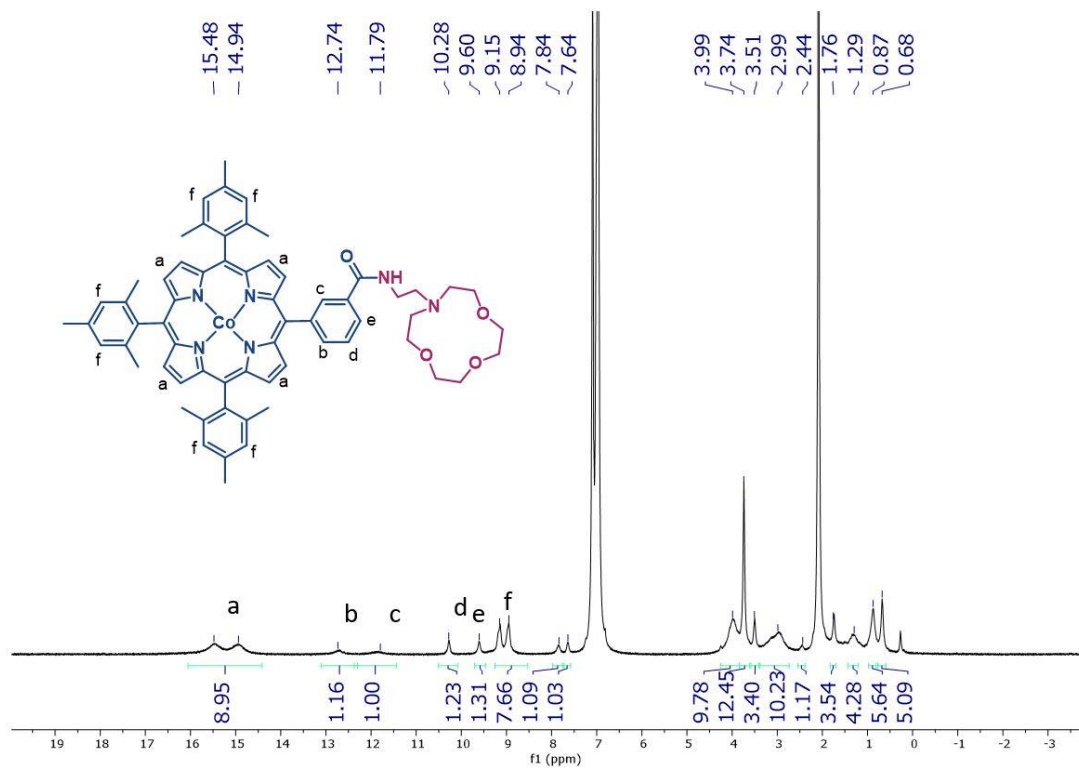


**Figure S4.** 400 MHz <sup>1</sup>H NMR spectrum of **1** in *d*<sub>8</sub>-toluene.

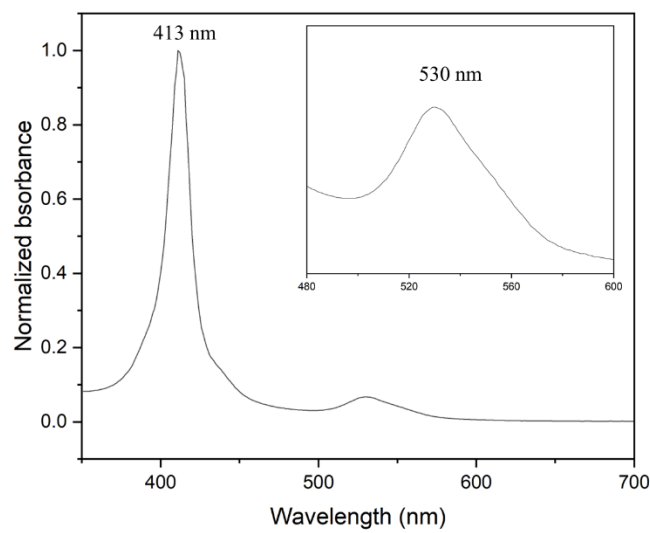


**Figure S5.** UV-vis spectrum of **1** in DCM.

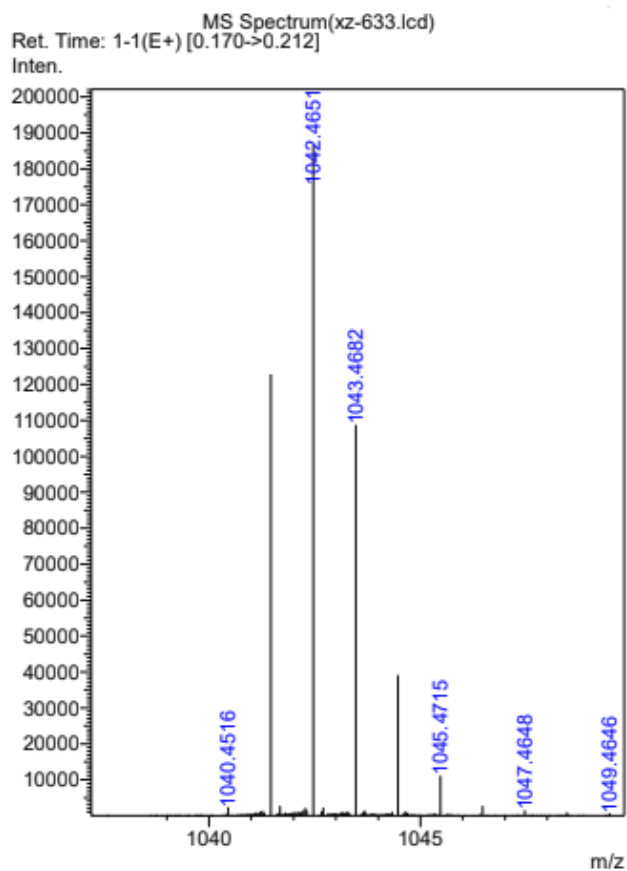


**Figure S6.** HRMS of **1**. Expected  $m/z$  ratios of the molecular-ion peaks are 1041.45 (100%), 1042.45 (72.3%), 1043.45 (26.0%), 1044.46 (6.1%), 1045.46 (1.1%).

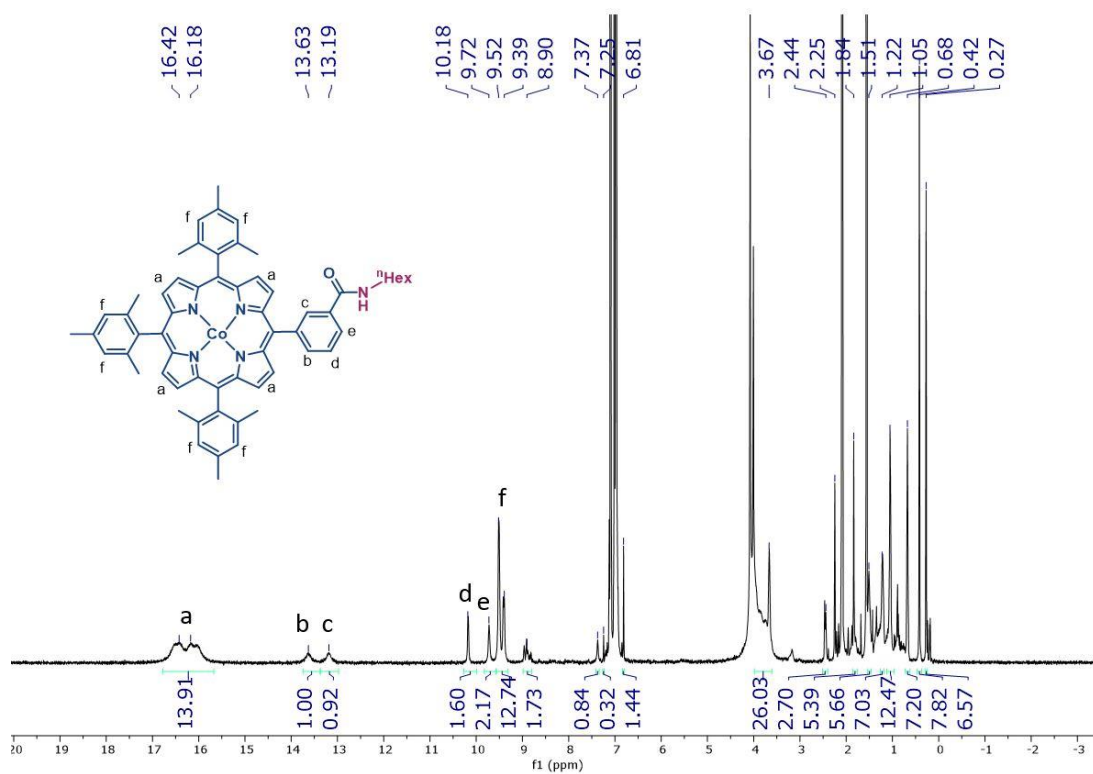


**Figure S7.** 400 MHz  $^1\text{H}$  NMR spectrum of **2** in  $d_8$ -toluene.

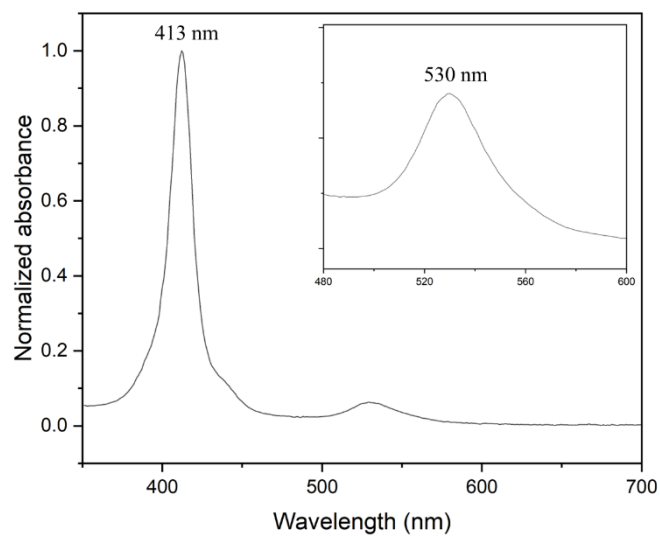


**Figure S8.** UV-vis spectrum of **2** in DCM.

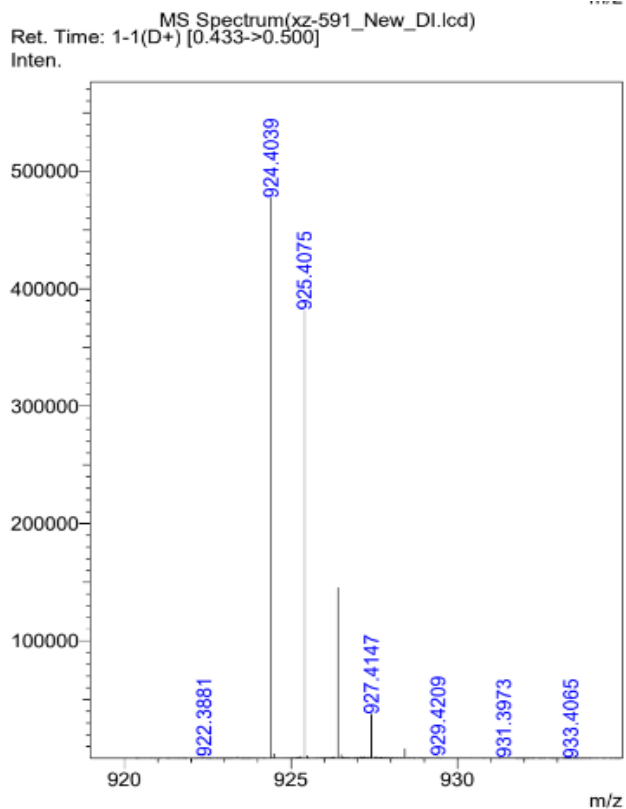


**Figure S9.** HRMS of **2**. Expected  $m/z$  ratios for the molecular-ion peaks are 924.41 (100%), 925.41 (67.4%), 926.41 (22.6%), 927.42 (4.5%).

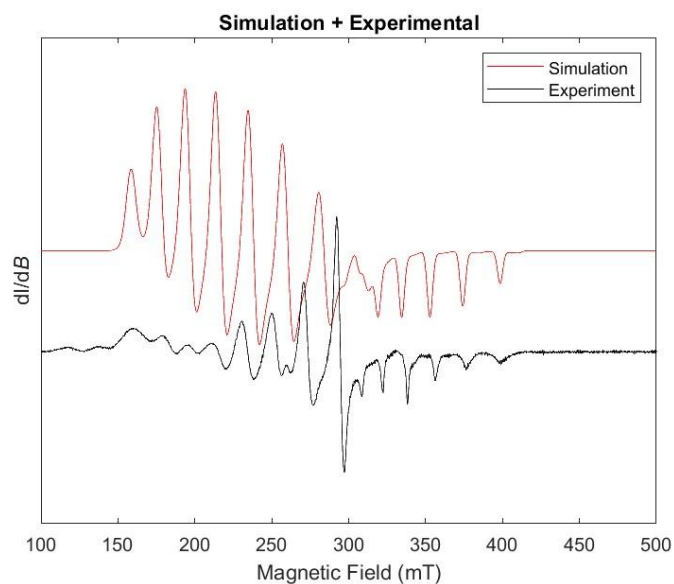


**Figure S10.** X-band EPR of **2** at 7 K in toluene.

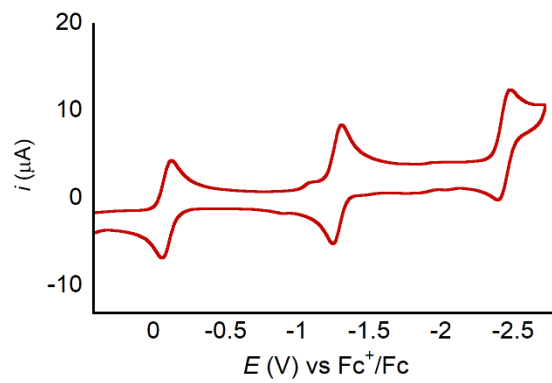


**Figure S11.** Cyclic voltammogram of 1 mM **2**, collected at 100 mV/s in 0.25 M TBAPF<sub>6</sub>/MeCN under Ar.

#### IV. Lewis Acid Binding to 1: HRMS

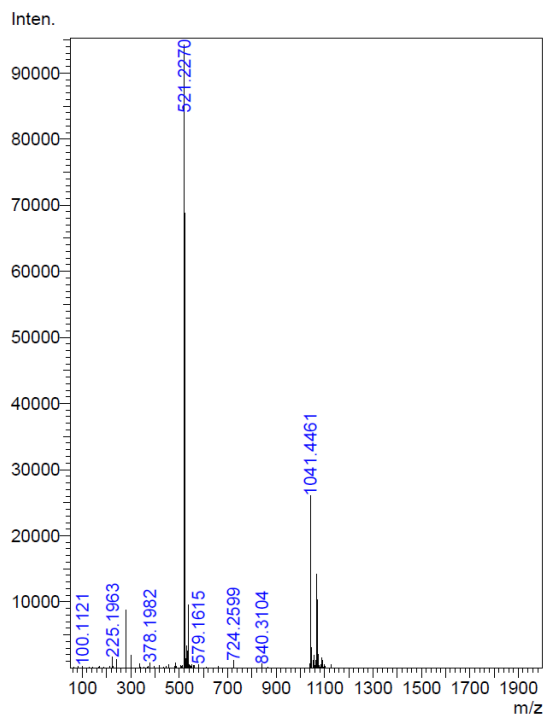


**Figure S12.** HRMS of **1** in MeCN, broad m/z window. Expected m/z ratios of the molecular-ion peaks are 1041.45 (100%), 1042.45 (72.3%), 1043.45 (26.0%), 1044.46 (6.1%), 1045.46 (1.1%). The peaks at and near 521.227 correspond to divalent molecular-ions.

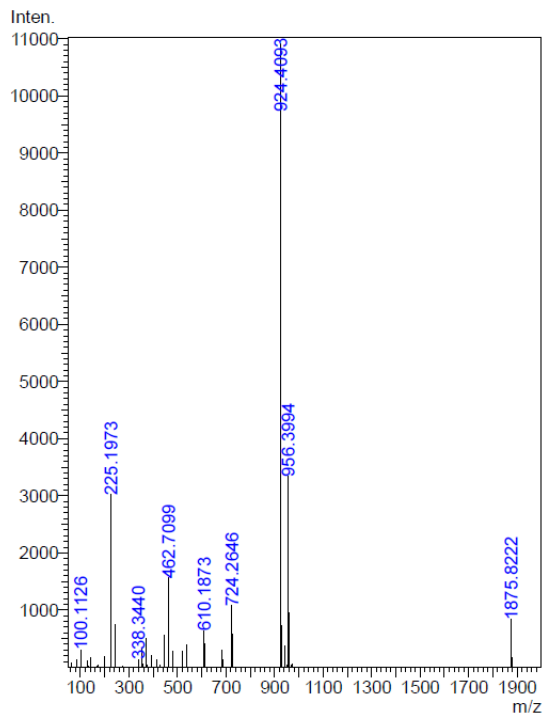


**Figure S13.** HRMS of **2** in MeCN, broad m/z window. HRMS of **2**. Expected m/z ratios for the molecular-ion peaks are 924.41 (100%), 925.41 (67.4%), 926.41 (22.6%), 927.42 (4.5%).

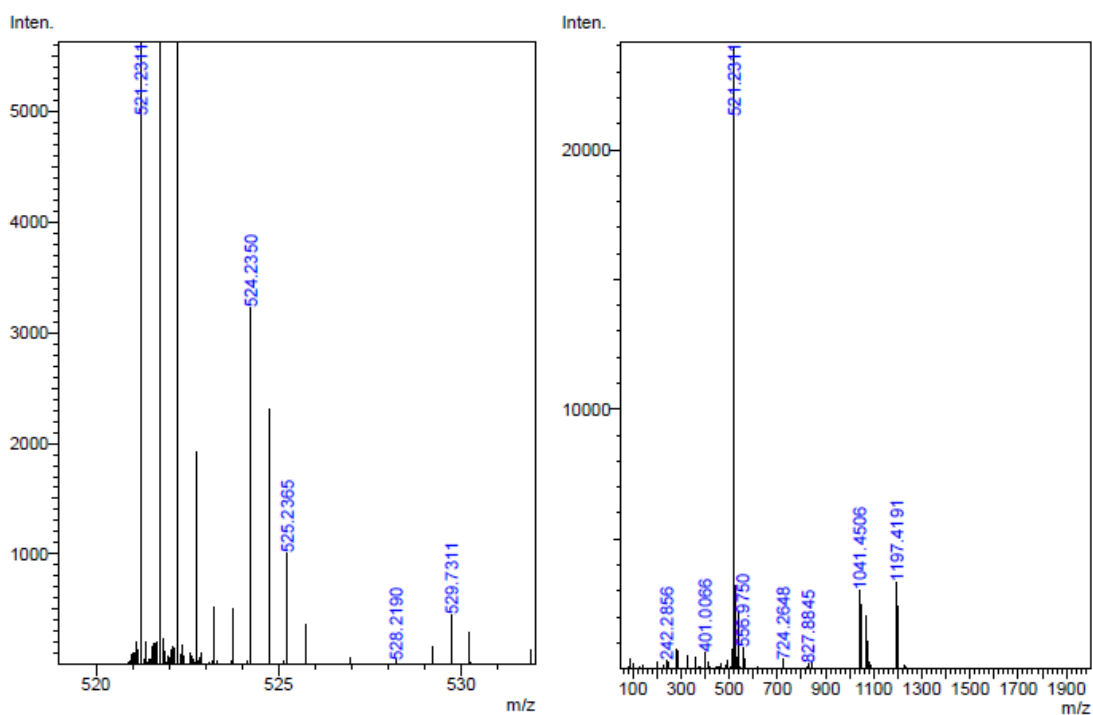


**Figure S14.** HRMS of **1** with added LiOTf (10 equiv) in MeCN. Relevant m/z peaks detected:  $[\mathbf{1-Li}]^+$  1048.47,  $[\mathbf{1-Li}]^{2+}$  524.24,  $[\mathbf{1-Li-OTf}]^+$  1197.42.

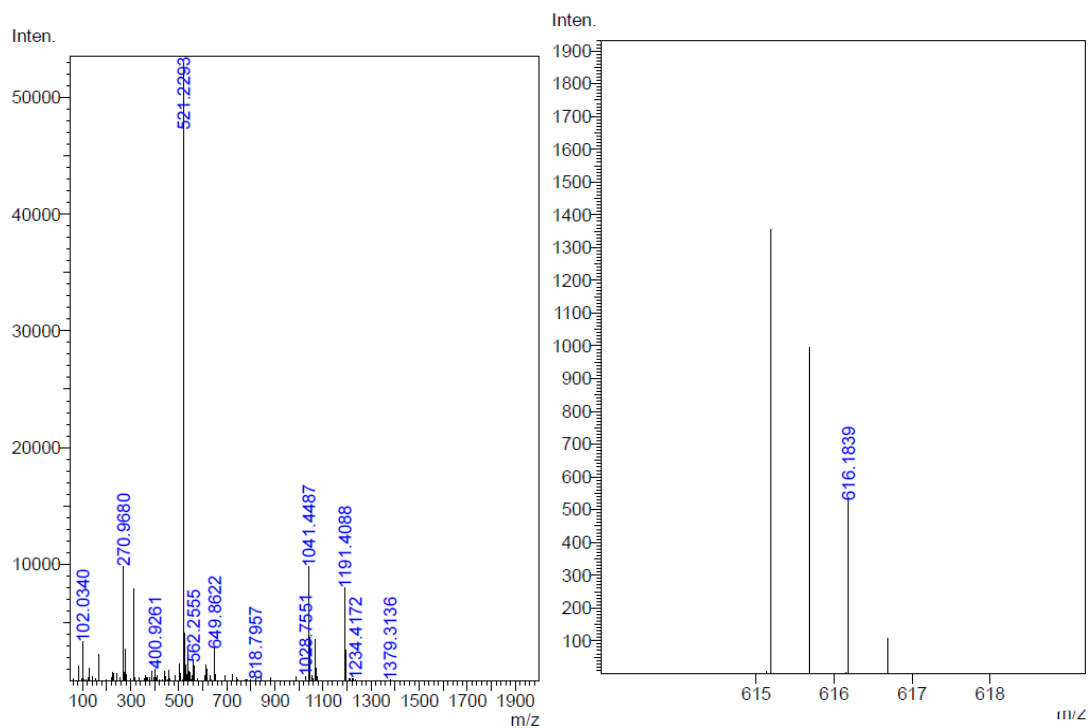


**Figure S15.** HRMS of **1** with added  $\text{Ca}(\text{OTf})_2$  (1 equiv) in MeCN. Relevant m/z peaks detected:  $[\mathbf{1-Ca-OTf}]^{2+}$  615.18.

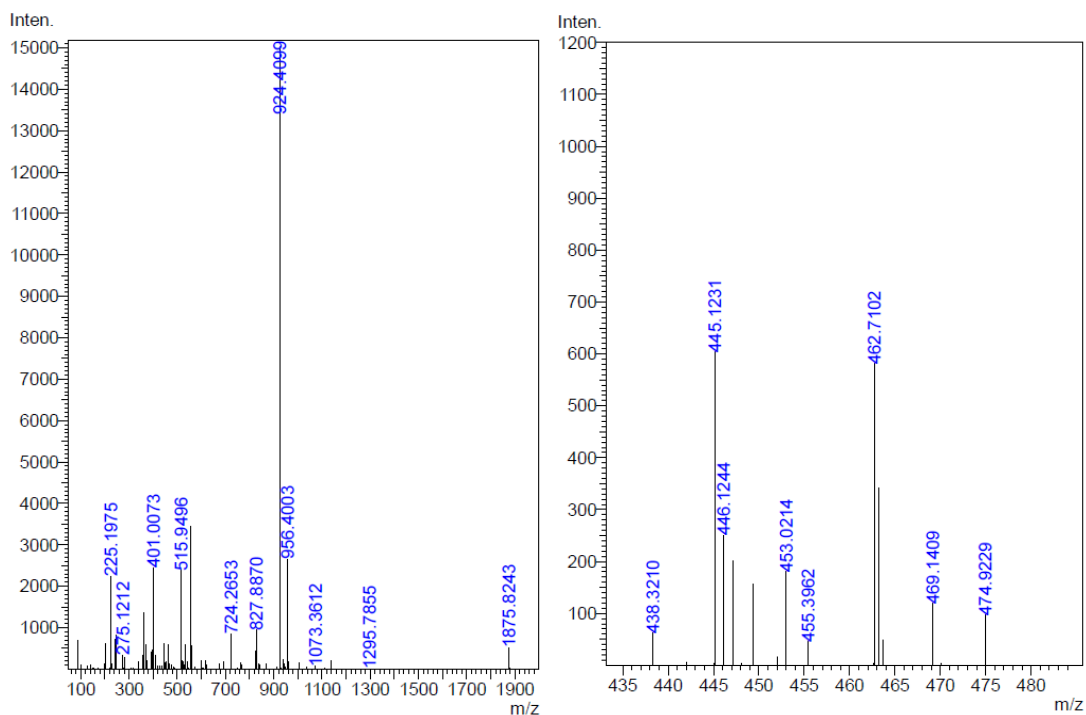


**Figure S16.** HRMS of **2** with added LiOTf (10 equiv) in MeCN. m/z peaks detected for complex **1** with Li<sup>+</sup> bound are absent in **2**: [2-Li]<sup>+</sup> 932.43, [2-Li]<sup>2+</sup> 466.22, [2-Li-OTf]<sup>+</sup> 1080.38.

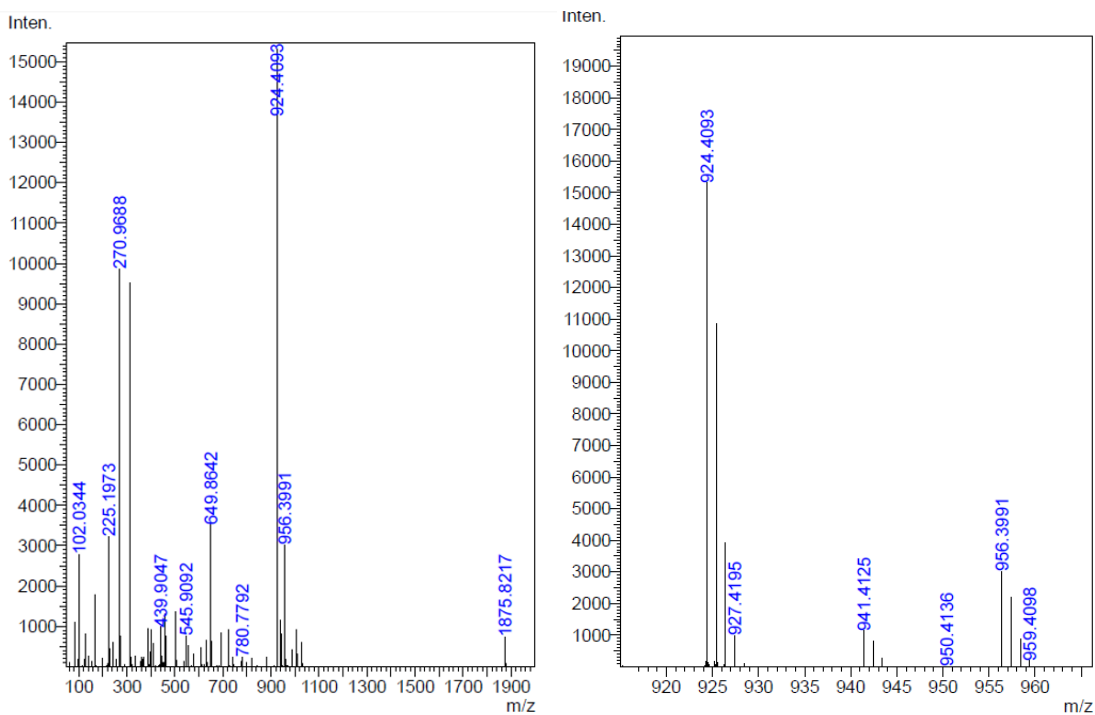


**Figure S17.** HRMS of **2** with added Ca(OTf)<sub>2</sub> (1 equiv) in MeCN. m/z peaks detected for complex **1** with Ca<sup>2+</sup> bound are absent in **2**: [2-Ca-OTf]<sup>2+</sup> 556.66.

## V. Lewis Acid Binding to 1: Variable Temperature $^7\text{Li}$ and $^{19}\text{F}$ NMR Spectroscopy

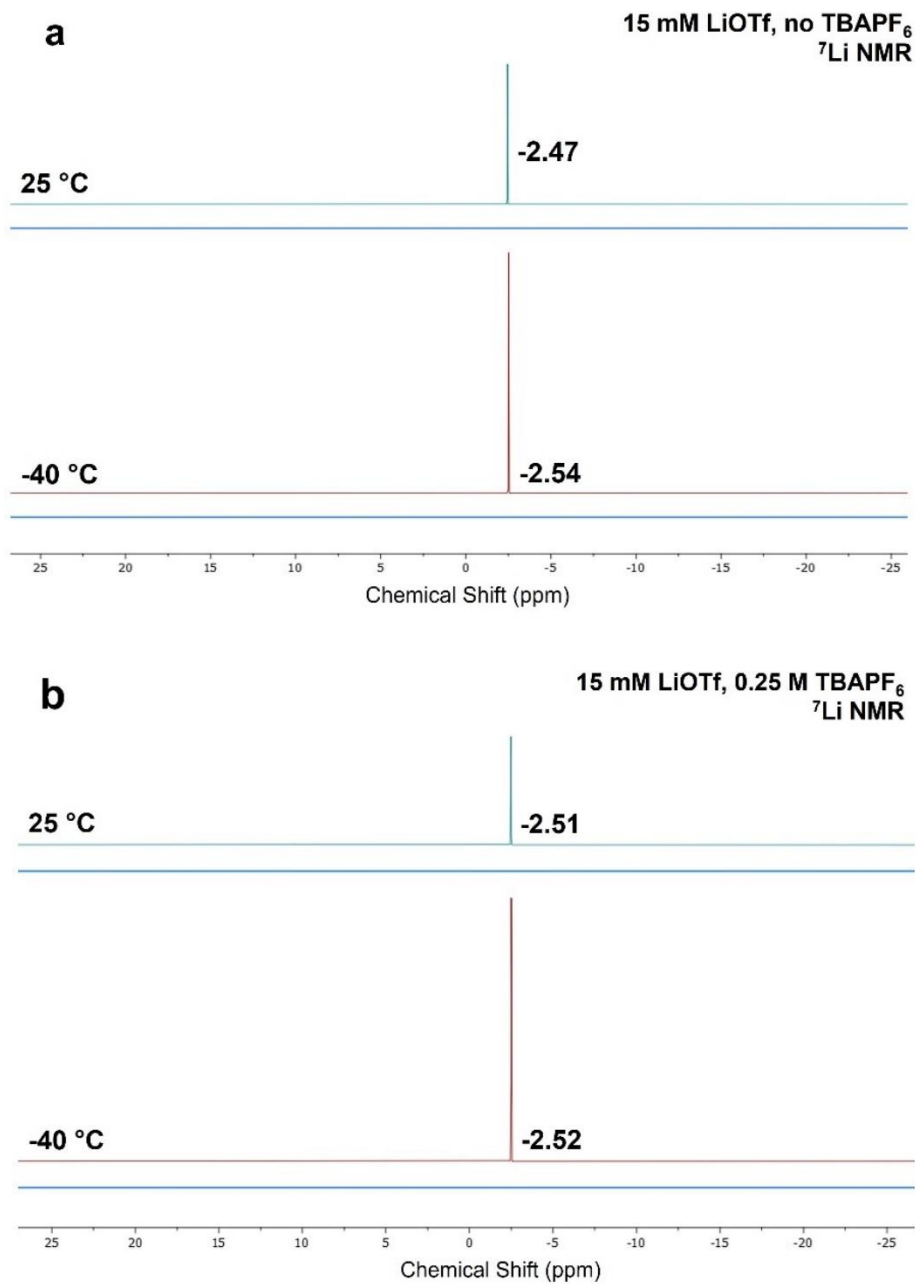


**Figure S18.** 194.36 MHz  $^7\text{Li}$  NMR spectra of 15 mM LiOTf in  $d_3\text{-MeCN}$  at 25 (top trace) and -40 °C (bottom trace) (a) with no added electrolyte and (b) with 0.25 M TBAPF<sub>6</sub>.

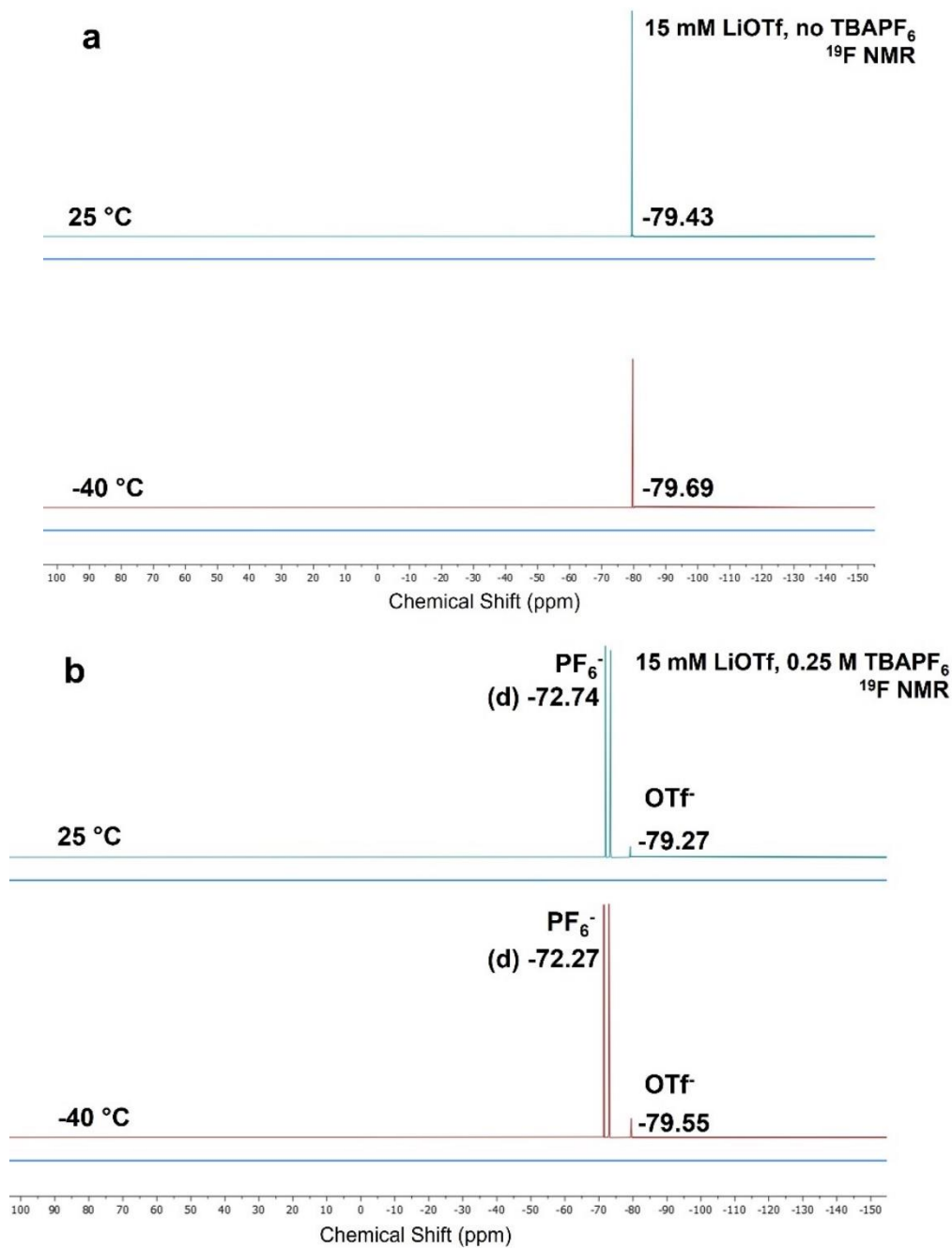


**Figure S19.** 470.56 MHz <sup>19</sup>F NMR spectra of 15 mM LiOTf in *d*<sub>3</sub>-MeCN at 25 (top trace) and -40 °C (bottom trace) (a) with no added electrolyte and (b) with 0.25 M TBAPF<sub>6</sub>.

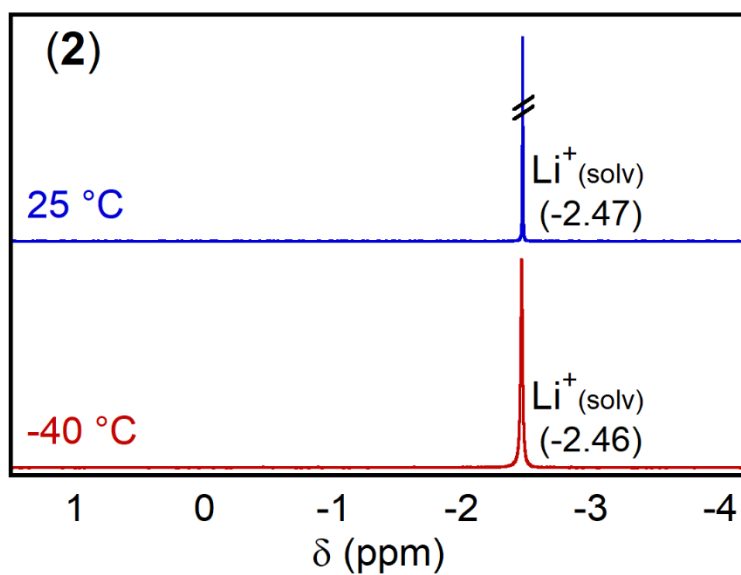


**Figure S20.** 194.36 MHz  ${}^7\text{Li}$  NMR spectra of 1.5 mM of **2** with added LiOTf (10 equiv) in  $d_3$ -MeCN containing 0.25 M TBAPF<sub>6</sub> at 25 (top trace) and -40 °C (bottom trace) in absence of TBAPF<sub>6</sub>. Figure 4b of the main text shows similar data collected in absence of TBAPF<sub>6</sub> electrolyte.

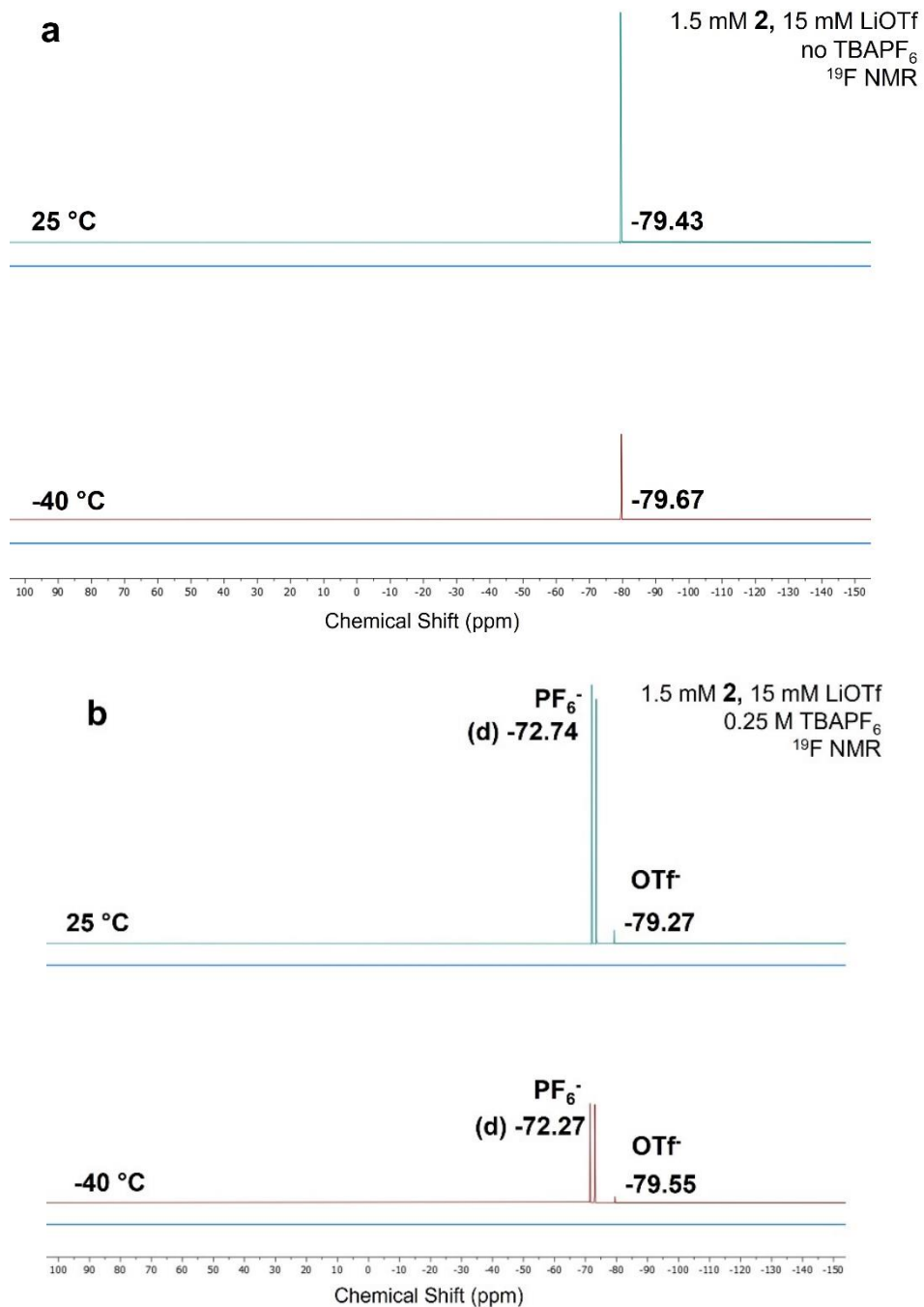


**Figure S21.** 470.56 MHz <sup>19</sup>F NMR spectra of 1.5 mM of **2** with added LiOTf (10 equiv) in d<sub>3</sub>-MeCN at 25 (top trace) and -40 °C (bottom trace) **(a)** with no added electrolyte and **(b)** with 0.25 M TBAPF<sub>6</sub>.

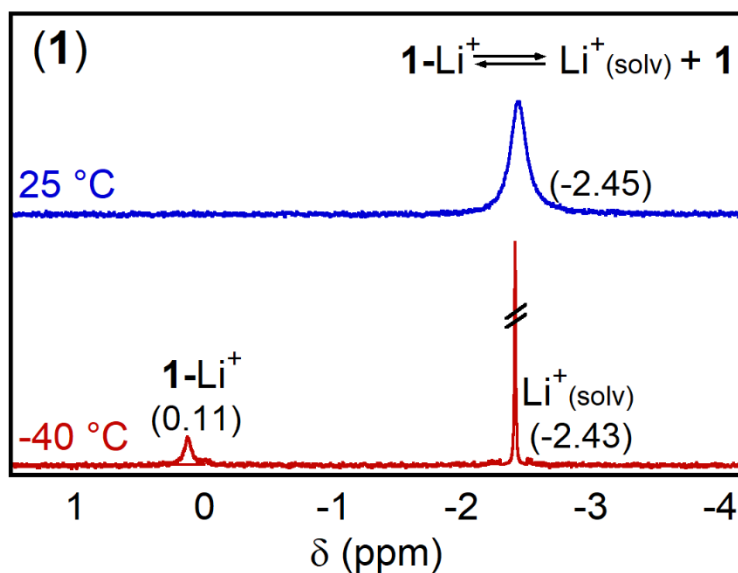


**Figure S22.** 194.36 MHz  $^7\text{Li}$  NMR spectra of 1.5 mM of **1** with added LiOTf (10 equiv) in  $d_3$ -MeCN containing 0.25 M TBAPF<sub>6</sub> at 25 (top trace) and -40 °C (bottom trace) in absence of TBAPF<sub>6</sub>. Figure 4a of the main text shows similar data collected in absence of TBAPF<sub>6</sub> electrolyte.

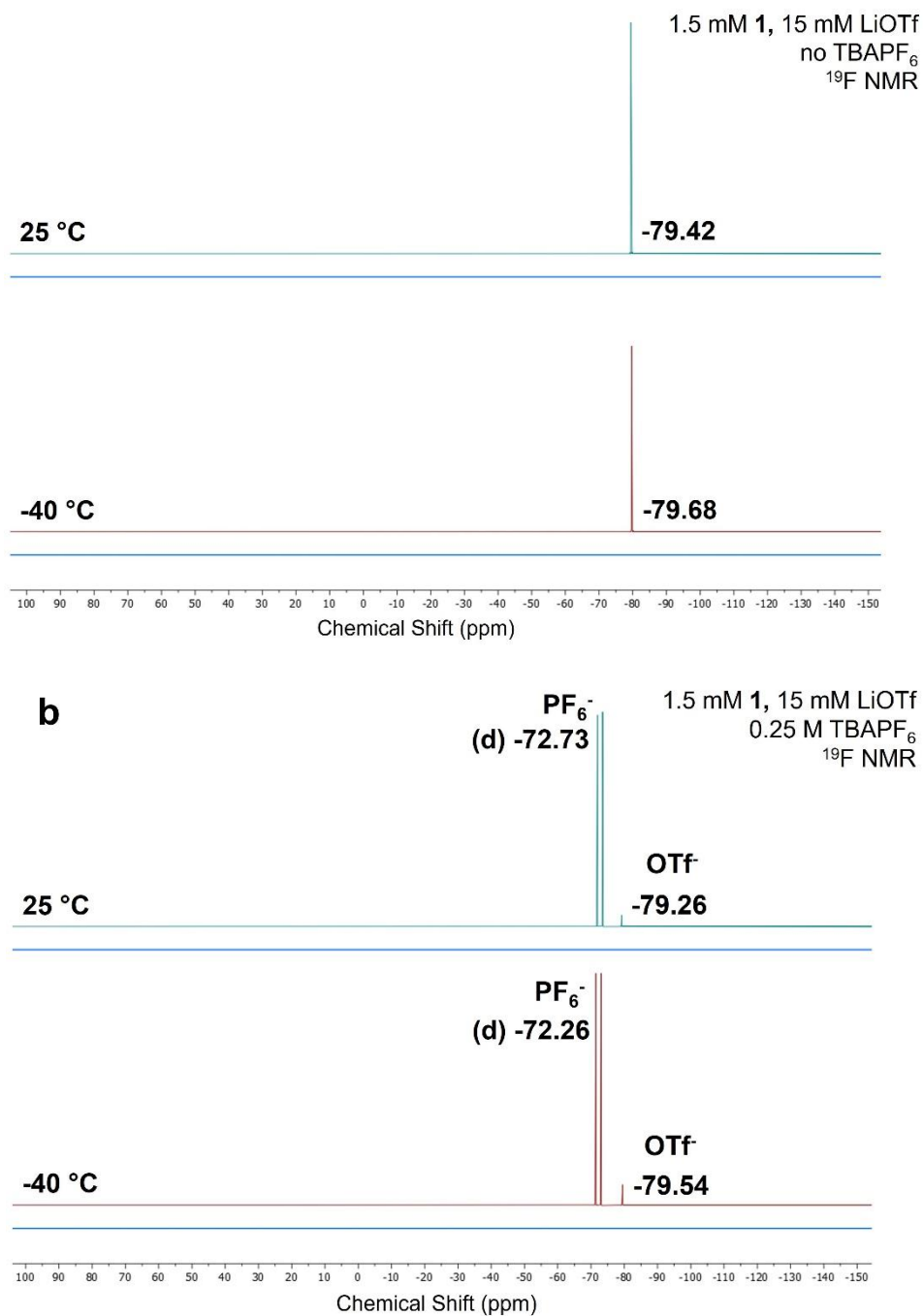


**Figure S23.** 470.56 MHz <sup>19</sup>F NMR spectra of 1.5 mM of **1** with added LiOTf (10 equiv) in d<sub>3</sub>-MeCN at 25 (top trace) and -40 °C (bottom trace) **(a)** with no added electrolyte and **(b)** with 0.25 M TBAPF<sub>6</sub>.

## VI. Li<sup>+</sup> Binding to **1**: <sup>7</sup>Li and <sup>1</sup>H NMR Spectroscopy, Job Plot

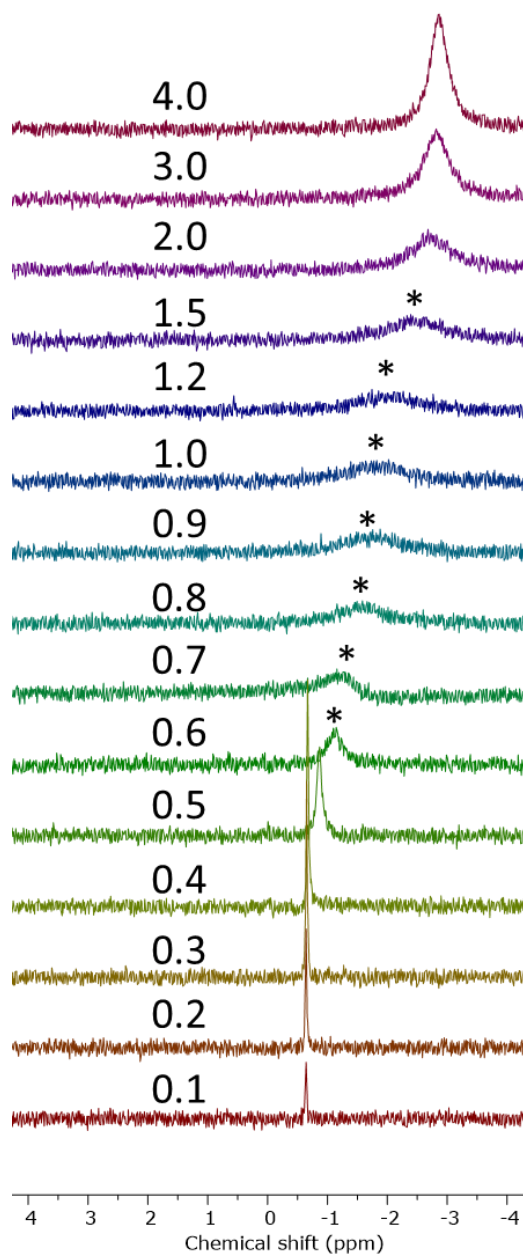


**Figure S24.** Chemical shift variation in the <sup>7</sup>Li NMR spectra upon adding increasing amounts of LiOTf to a solution containing 1.5 mM of **1** in *d*<sub>3</sub>-MeCN with 0.25 M TBAPF<sub>6</sub>. The molar equivalents of LiOTf relative to **1** are shown in the figure. Similar data collected in the absence of 0.25 M TBAPF<sub>6</sub> electrolyte in solution is presented in Figure 5 of the main text.

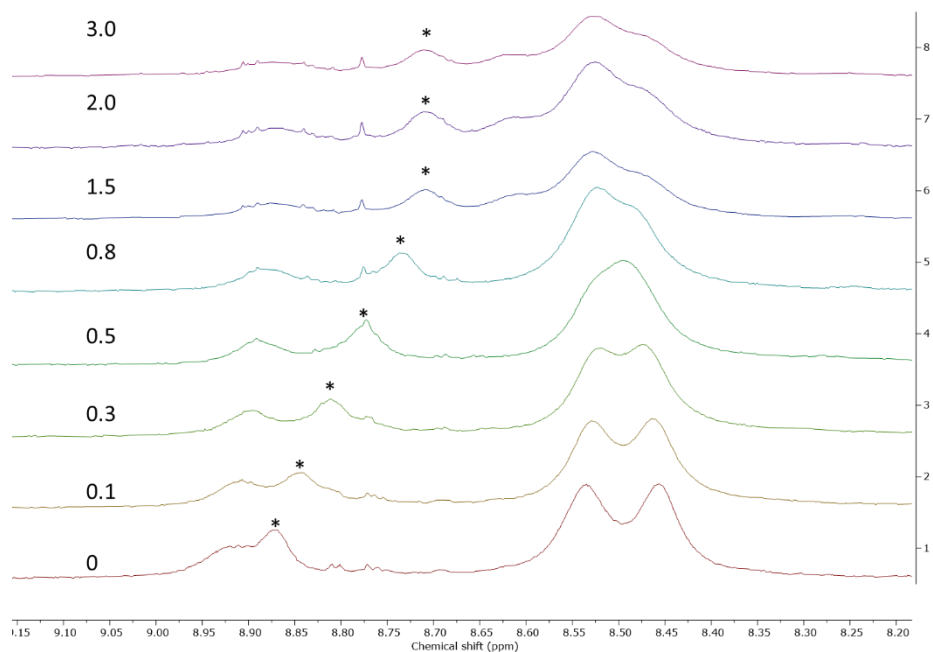


**Figure S25.** Chemical shift variation in the <sup>1</sup>H NMR peaks that proved more sensitive to addition of LiOTf in a 1.5 mM solution of **1** in *d*<sub>3</sub>-MeCN with 0.25 M TBAPF<sub>6</sub>. The molar equivalents of LiOTf relative to **1** are shown in the figure, the peak marked with \*, initially at 8.87 ppm, was used to generate the Job plot.

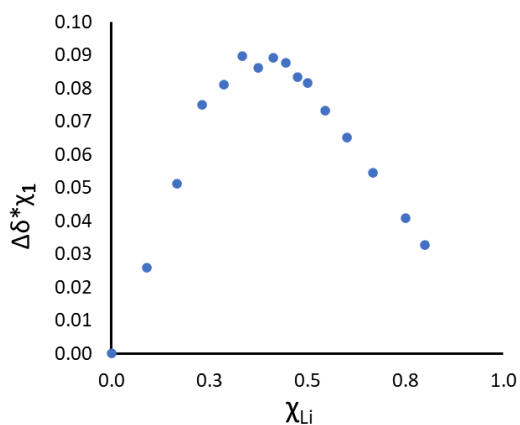


**Figure S26.** Job plots obtained from the <sup>1</sup>H NMR data shown in Figure S25 for the peak initially centered at 8.80 ppm from the titration of **1** with LiOTf with 0.25 M TBAPF<sub>6</sub>.

## VII. Determination of Binding Constants: Nonlinear Fitting

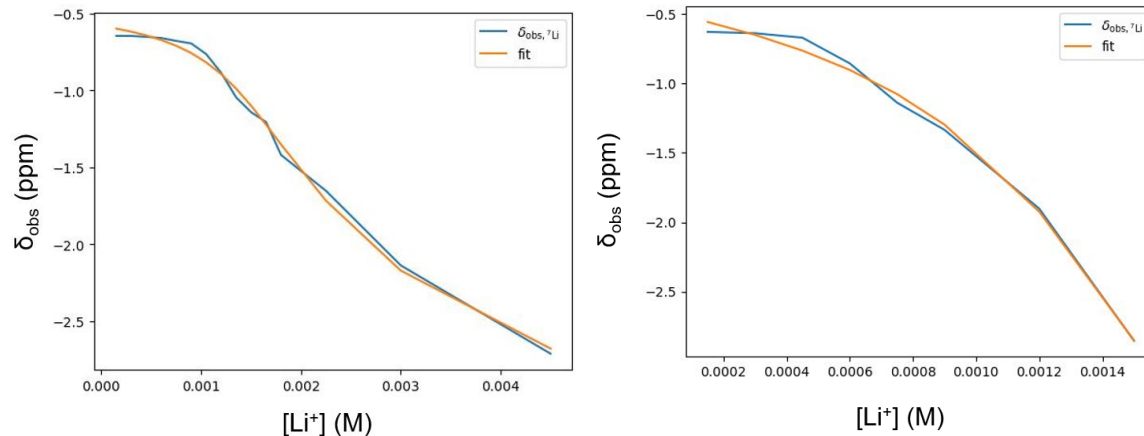


**Figure S27.** Nonlinear fitting of eq. 2 of the main text to determine the binding constant of  $\text{Li}^+$  to **1**. **(left)**  $^7\text{Li}$  NMR data collected with 0.25 M  $\text{TBAPF}_6$  in  $d_3$ -MeCN, fitting results were  $K_b = 1.309 \pm 0.299 \times 10^4 \text{ M}^{-1}$ ,  $\delta_{\text{Li}} = -2.57 \pm 0.05$  ppm, and  $\delta_{\text{ML}} = -0.41 \pm 0.06$  ppm. **(right)**  $^7\text{Li}$  NMR data collected in  $d_3$ -MeCN with no added  $\text{TBAPF}_6$  electrolyte, fitting results were  $K_b = 1.212 \pm 0.257 \times 10^4 \text{ M}^{-1}$ ,  $\delta_{\text{Li}} = -3.66 \pm 0.06$  ppm, and  $\delta_{\text{ML}} = -0.42 \pm 0.06$  ppm.

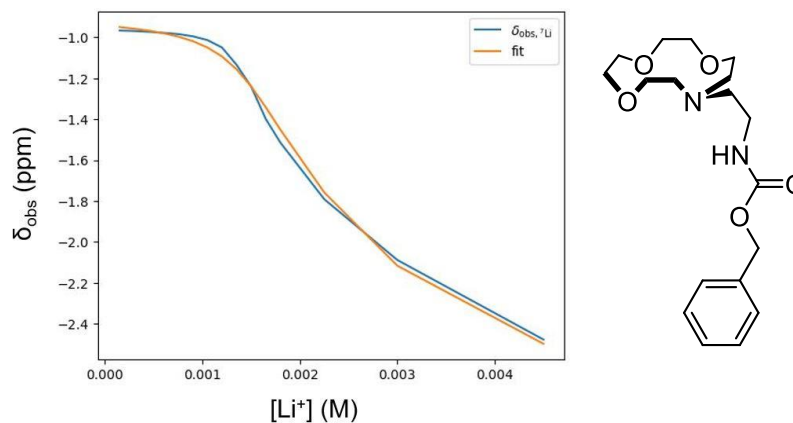


**Figure S28.** Nonlinear fitting of eq. 2 of the main text for the binding of  $\text{Li}^+$  to a structurally related free aza-crown based on  $^7\text{Li}$  NMR data, fitting results were  $K_b = 2.579 \pm 0.607 \times 10^4 \text{ M}^{-1}$ ,  $\delta_{\text{Li}} = -3.29 \pm 0.04$  ppm, and  $\delta_{\text{ML}} = -0.88 \pm 0.03$  ppm.

### VIII. Li<sup>+</sup> Binding to Free Crown: <sup>7</sup>Li and <sup>1</sup>H NMR Spectroscopy, Job Plot

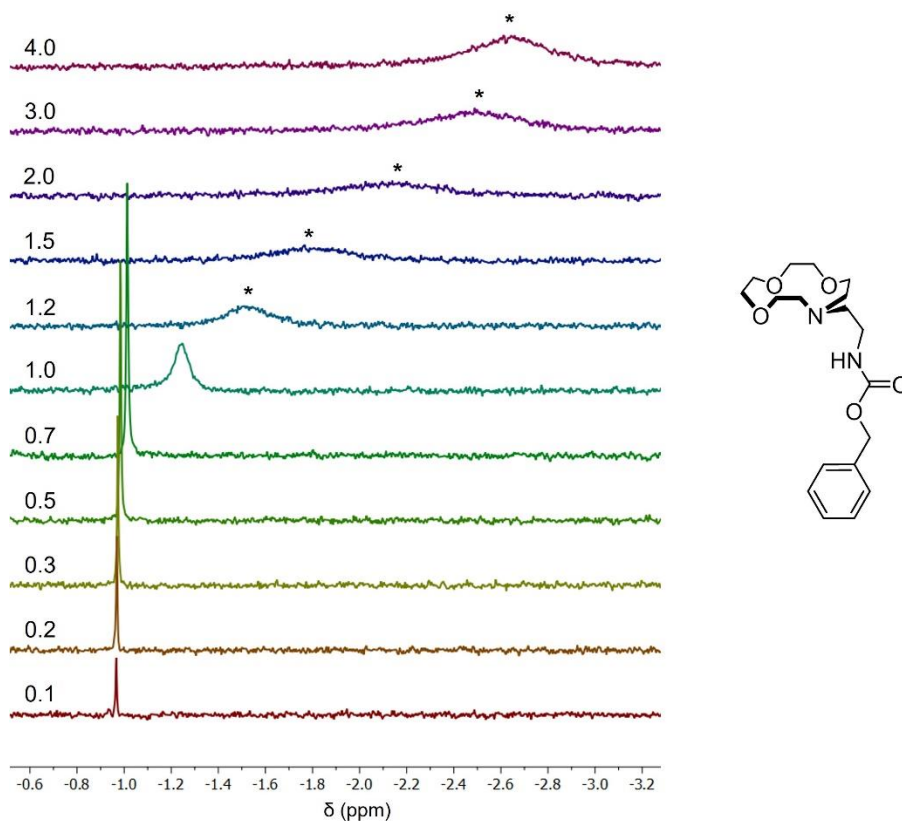


**Figure S29.** (left) Chemical shift variation in the <sup>7</sup>Li NMR spectra upon adding increasing amounts of LiOTf to a solution containing 1.5 mM of free crown in *d*<sub>3</sub>-MeCN. The molar equivalents of LiOTf relative to crown are shown in the figure. (right) The structure of the free crown used in this study, which was synthesized as reported elsewhere.<sup>12</sup>

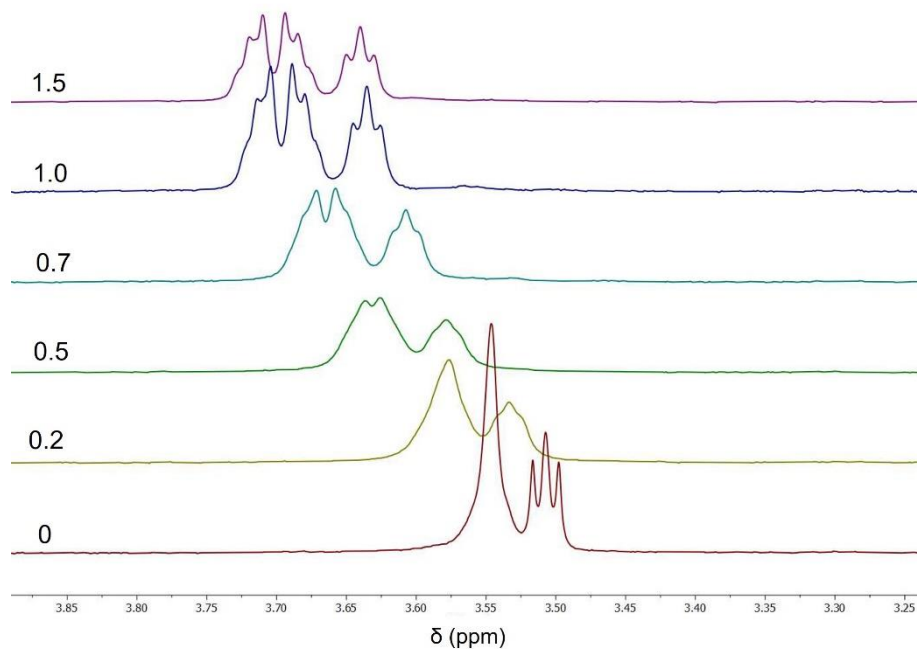


**Figure S30.** Chemical shift variation in the  $^1\text{H}$  NMR peaks corresponding to protons in the crown, upon adding increasing amounts of LiOTf to a solution containing 1.5 mM of free crown in  $d_3$ -MeCN. The molar equivalents of LiOTf relative to crown are shown in the figure. The triplet centered at 3.51 ppm is used to generate the Job plot.

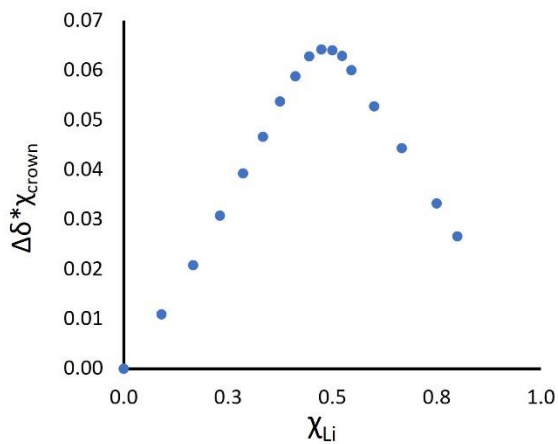


**Figure S31.** Job plot obtained from the  $^1\text{H}$  NMR peak initially centered at 3.51 ppm showing a maximum near a Li molar fraction ( $\chi_{\text{Li}}$ ) of 0.5 indicating formation of a 1:1 adduct between Li and free crown.

### VIII. Other Lewis Acids Binding to **1**: Titrations monitored by $^1\text{H}$ NMR Spectroscopy

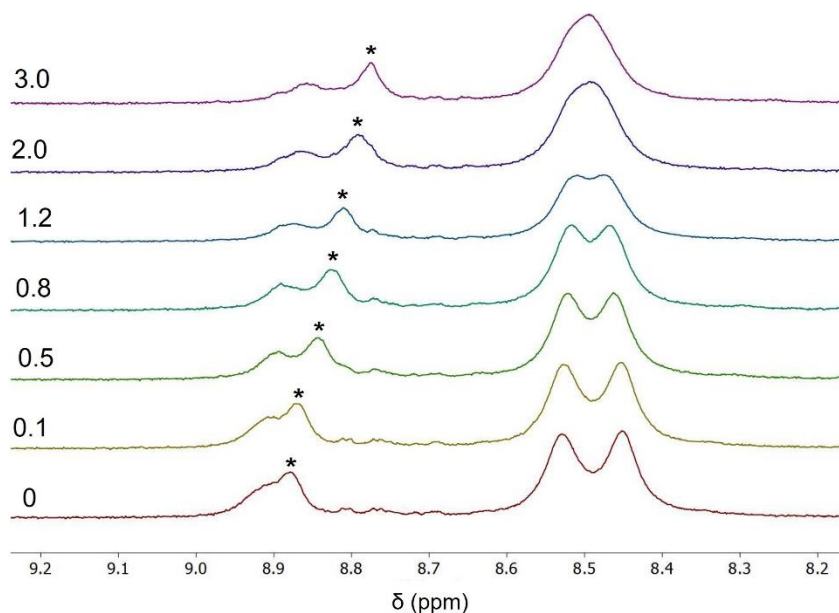


**Figure S32.** Chemical shift variation in the  $^1\text{H}$  NMR peaks that change chemical shift upon addition of NaOTf in a 1.5 mM solution of **1** in  $d_3$ -MeCN. The molar equivalents of NaOTf relative to **1** are shown in the figure, the peak marked with \* was used to generate the Job plot.

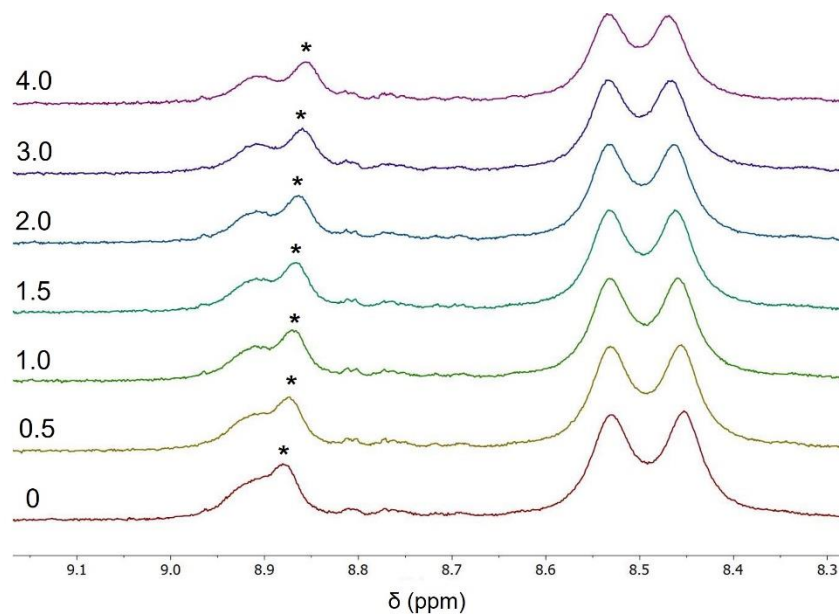


**Figure S33.** Chemical shift variation in the  $^1\text{H}$  NMR peaks that change chemical shift upon addition of KOTf in a 1.5 mM solution of **1** in  $d_3$ -MeCN. The molar equivalents of KOTf relative to **1** are shown in the figure, the peak marked with \* was used to generate the Job plot.

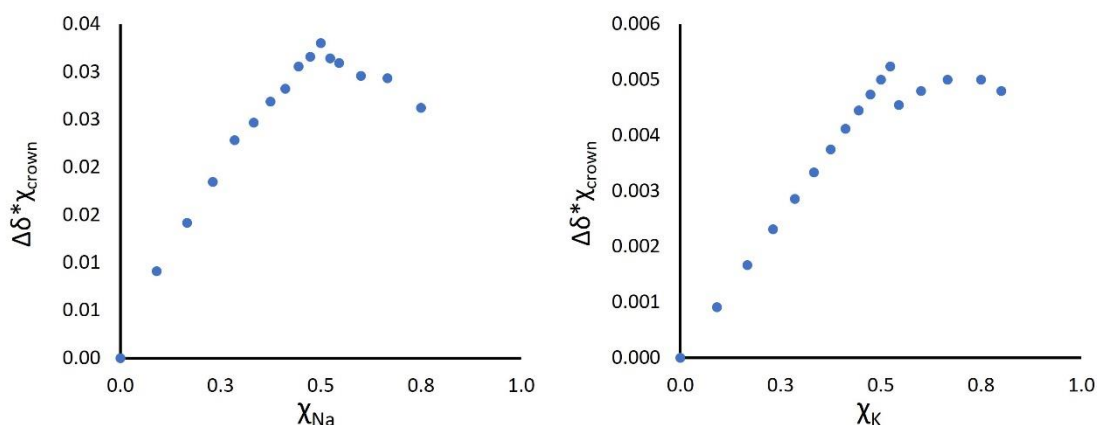


**Figure S34.** Job plots obtained from the  $^1\text{H}$  NMR peak initially centered at 8.80 ppm showing a maximum near a LA molar fraction ( $\chi_{\text{Li}}$ ) of 0.5 indicating formation of a 1:1 adduct between LA and **1**. (left) NaOTf and (right) KOTf. The changes in chemical shifts seen in the  $^1\text{H}$  NMR spectra of **1** with increasing concentrations of NaOTf and KOTf are relatively small relative to those seen with LiOTf, affecting the quality of the Job plots.

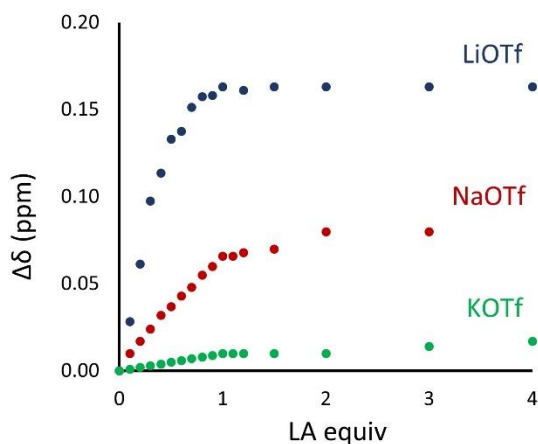


**Figure S35.** Plot of the change in  $^1\text{H}$  NMR chemical shift for the peak initially at 8.88 ppm vs the equivalents of LA salt added to **1**. Spectra collected in a 1.5 mM solution of **1** in  $d_3$ -MeCN with increasing amounts of LAOTf.

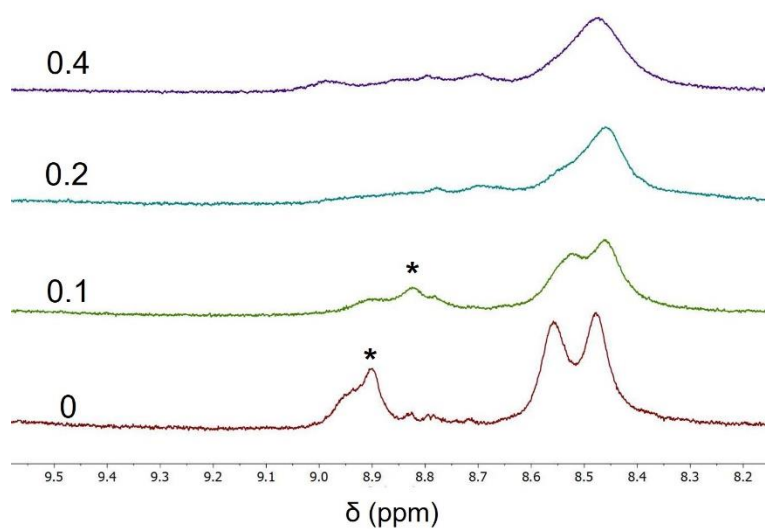


**Figure S36.** Chemical shift variation in the <sup>1</sup>H NMR peaks that change chemical shift upon addition of Ca(OTf)<sub>2</sub> in a 1.5 mM solution of **1** in *d*<sub>3</sub>-MeCN. The molar equivalents of Ca(OTf)<sub>2</sub> relative to **1** are shown in the figure. When further equivalents of Ca(OTf)<sub>2</sub> are added the peak broadens into the baseline.

## IX. Cyclic Voltammograms in the Presence of TBAOTf

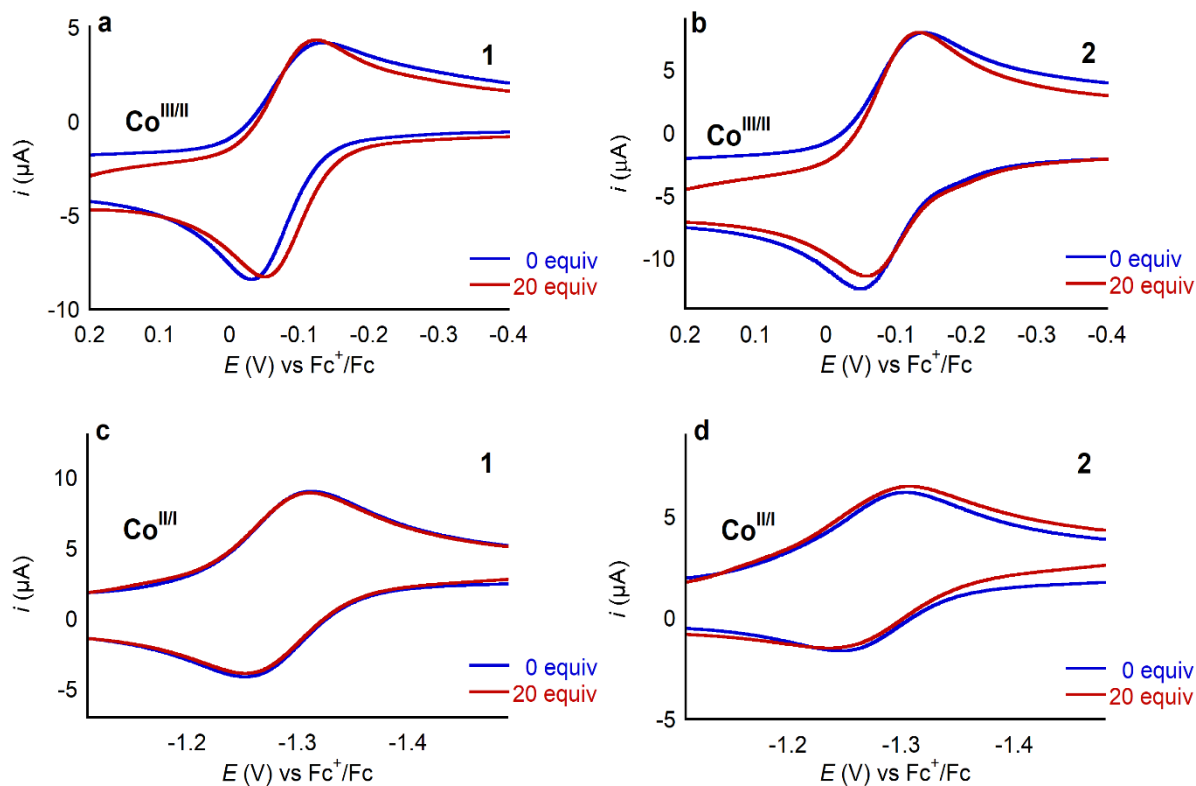


**Figure S37.** Cyclic voltammograms of the Co(III)/Co(II) (a) & (b) and Co(II)/Co(I) (c) & (d) couples of **1** and **2**, respectively, in absence of and upon adding 20 equivalents of TBAOTf, showing that the presence of triflate anions does not impact the Co(II)/Co(I) couple of **1** and only small changes are seen in the Co(III)/Co(II) couple. Cyclic voltammograms were collected at 100 mV/s in 0.25 M TBAPF<sub>6</sub> in MeCN containing 0.5 mM of complex **1** under Ar.

## X. Cyclic Voltammograms in the Presence of Lewis Acids

**Table S2.** Summary of potential shift ( $\Delta E_{1/2}$ ) seen for the Co(II)/Co(I) couple of complexes **1** and **2** when different cationic Lewis acids ( $LA^+$ ) are present. A deviation of 3 mV is determined as the error from three independent CV experiments performed for complex **1** with added  $Ca(OTf)_2$ .

$LA^+$	Equiv. of $LA^+$ relative to CoPor	$\Delta E_{1/2}$ Co(II/I) (mV)	
		<b>1</b> (CoPor- $O_3N$ crown) ( $\pm 3$ mV)	<b>2</b> (CoPor-NHex)
$Ca^{2+}$	1	34	1
$Sr^{2+}$	1	36	-1
$Ba^{2+}$	2	25	-1
$Li^+$	10	15	1
$Na^+$	12	12	0
$K^+$	18	8	2

**Table S3.** Summary of peak potentials ( $E_p$ ) for individual reduction (red) and oxidation (ox) features, as well as half-peak potential ( $E_{1/2}$ ) corresponding to the Co(II)/Co(I) and Co(III)/Co(II) couples of complex **1** with and without Lewis acids (LA) present.

LA	<b>1</b> $E$ Co(II/I) (V) vs $Fc^+/Fc$			<b>1</b> $E$ Co(III/II) (V) vs $Fc^+/Fc$		
	$E_p$ red	$E_p$ ox	$E_{1/2}$	$E_p$ red	$E_p$ ox	$E_{1/2}$
$Ca^{2+}$	-1.279	-1.218	-1.248	-0.122	0.049	-0.036
no $Ca^{2+}$	-1.313	-1.251	-1.282	-0.125	-0.044	-0.084
$Sr^{2+}$	-1.289	-1.226	-1.258	-0.100	0.075	-0.013
no $Sr^{2+}$	-1.327	-1.261	-1.294	-0.140	0.042	-0.049
$Ba^{2+}$	-1.291	-1.232	-1.261	-0.133	0.009	-0.062
no $Ba^{2+}$	-1.316	-1.255	-1.286	-0.133	-0.049	-0.091
$Li^+$	-1.299	-1.236	-1.267	-0.138	-0.029	-0.083
no $Li^+$	-1.311	-1.253	-1.282	-0.133	-0.044	-0.089
$Na^+$	-1.300	-1.242	-1.271	-0.137	-0.030	-0.084
no $Na^+$	-1.313	-1.254	-1.255	-0.139	-0.039	-0.089
$K^+$	-1.302	-1.246	-1.274	-0.142	-0.032	-0.086
no $K^+$	-1.310	-1.254	-1.282	-0.140	-0.033	-0.087

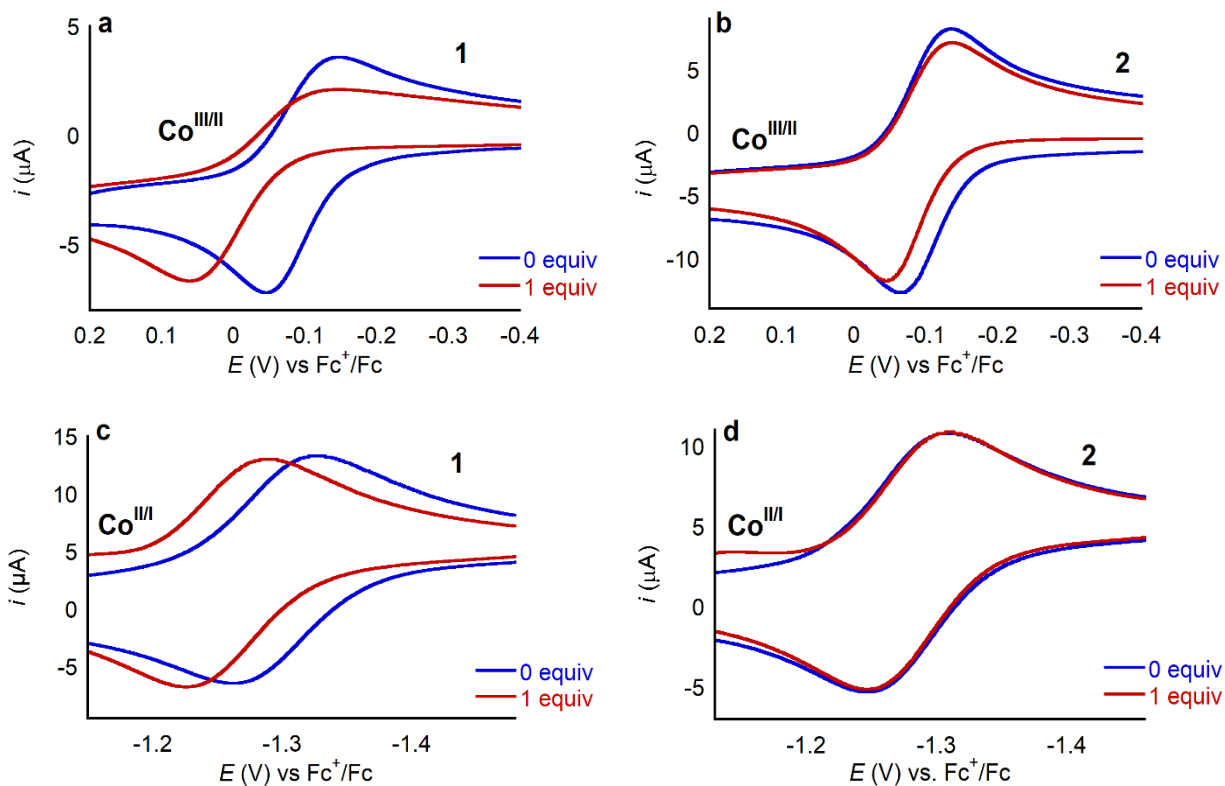


**Figure S38.** Cyclic voltammograms of the  $\text{Co}(\text{III})/\text{Co}(\text{II})$  (a) & (b) and  $\text{Co}(\text{II})/\text{Co}(\text{I})$  (c) & (d) couples of **1** and **2**, respectively, in absence of LA and upon addition of 1 equivalent of  $\text{Sr}(\text{OTf})_2$ , showing that only for **1** the added LA impacts the CV response. Cyclic voltammograms were collected at 100 mV/s in 0.25 M  $\text{TBAPF}_6$  in MeCN containing 0.5 mM of complex **1** under Ar.

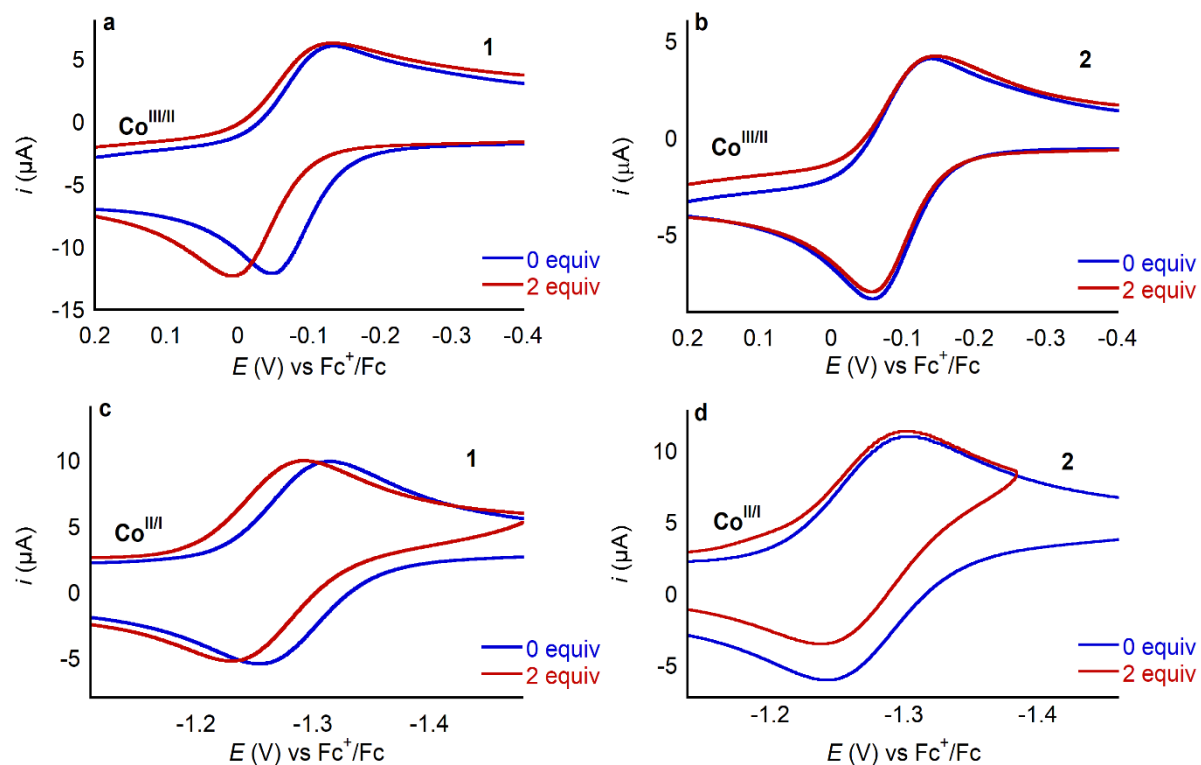


**Figure S39.** Cyclic voltammograms of the Co(III)/Co(II) (a) & (b) and Co(II)/Co(I) (c) & (d) couples of **1** and **2**, respectively, in absence of LA and upon addition of 2 equivalents of Ba(OTf)<sub>2</sub>, showing that only for **1** the added LA impacts the CV response. Cyclic voltammograms were collected at 100 mV/s in 0.25 M TBAPF<sub>6</sub> in MeCN containing 0.5 mM of complex **1** under Ar.

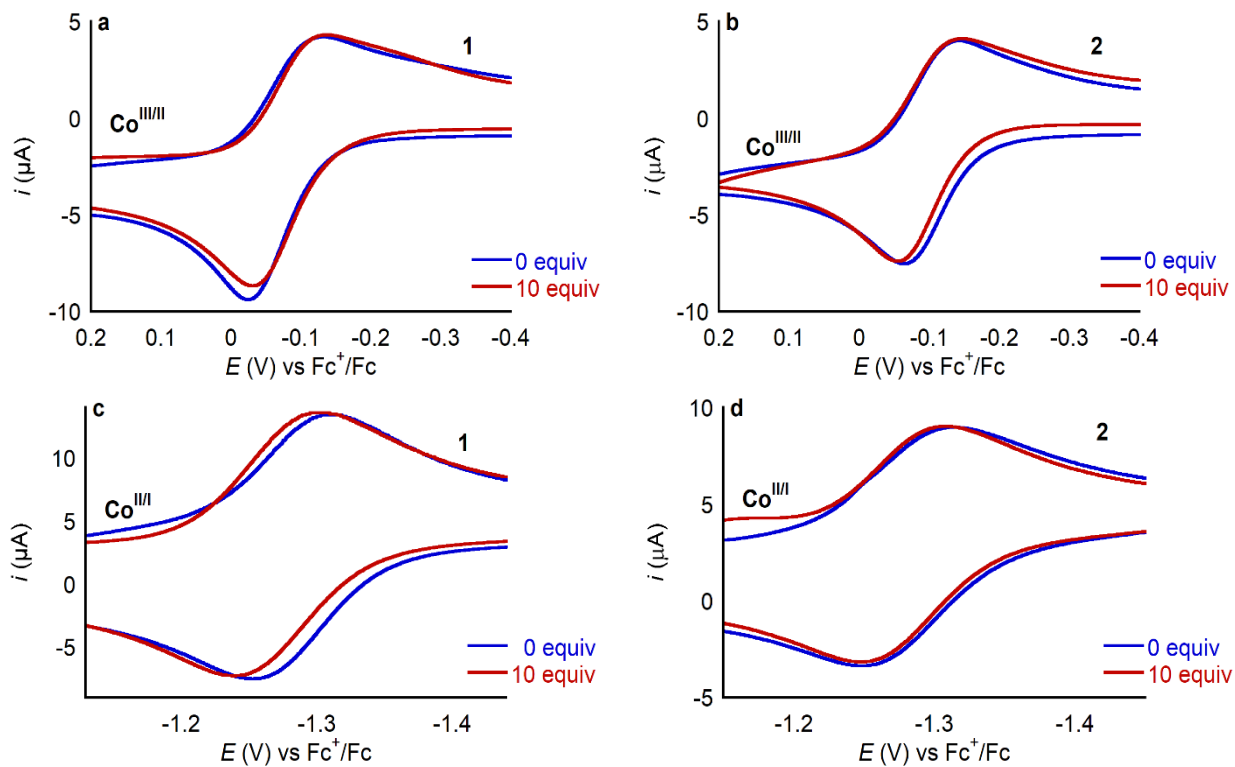


**Figure S40.** Cyclic voltammograms of the  $\text{Co}^{\text{III/II}}$  (a) & (b) and  $\text{Co}^{\text{II/I}}$  (c) & (d) couples of **1** and **2**, respectively, in absence of LA and upon addition of 10 equivalent of LiOTf, showing that only for **1** the added LA impacts the CV response. Cyclic voltammograms were collected at 100 mV/s in 0.25 M  $\text{TBAPF}_6$  in MeCN containing 0.5 mM of complex **1** under Ar.

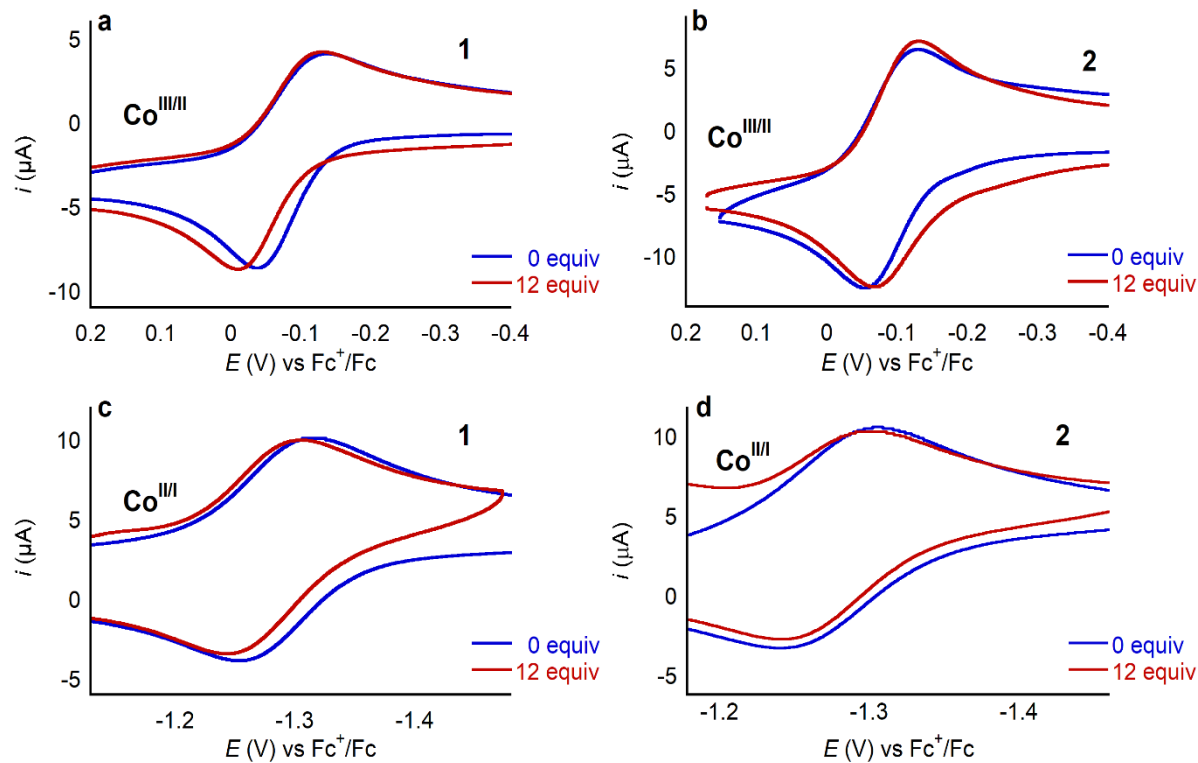


**Figure S41.** Cyclic voltammograms of the Co(III)/Co(II) (a) & (b) and Co(II)/Co(I) (c) & (d) couples of **1** and **2**, respectively, in absence of LA and upon addition of 12 equivalents of NaOTf, showing that only for **1** the added LA impacts the CV response. Cyclic voltammograms were collected at 100 mV/s in 0.25 M TBAPF<sub>6</sub> in MeCN containing 0.5 mM of complex **1** under Ar.

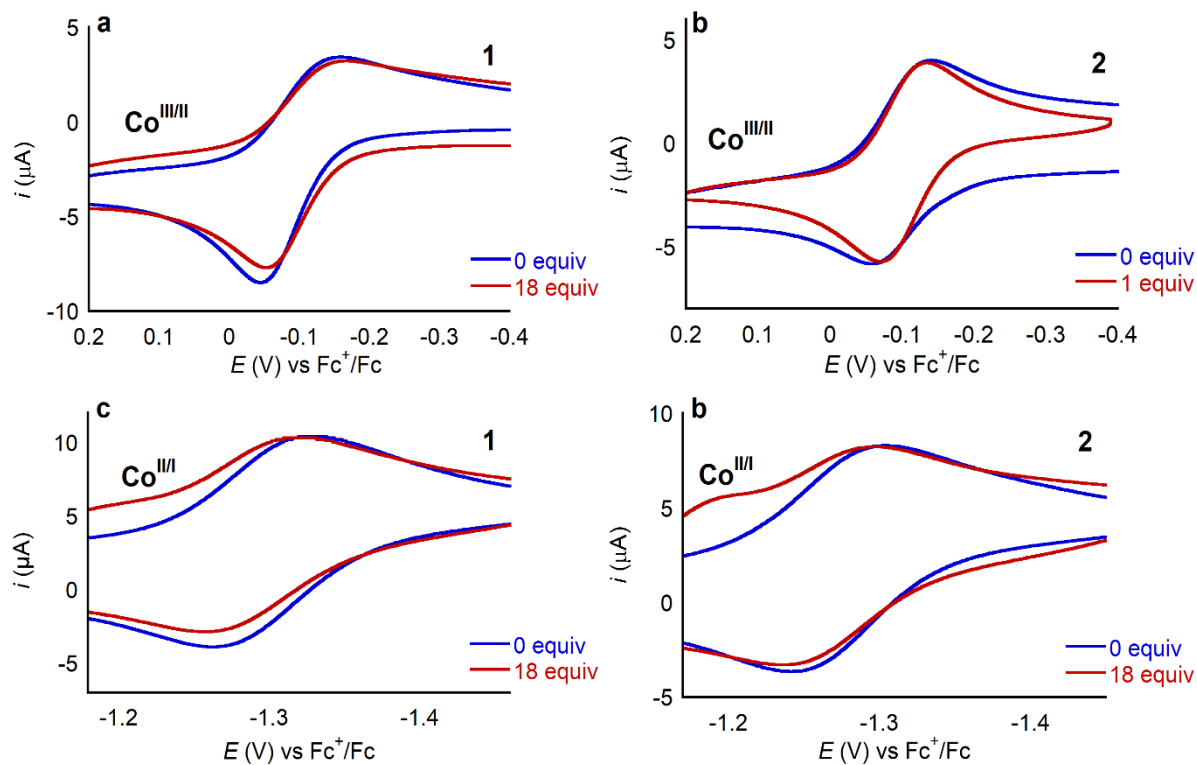


**Figure S42.** Cyclic voltammograms of the Co(III)/Co(II) (a) & (b) and Co(II)/Co(I) (c) & (d) couples of **1** and **2**, respectively, in absence of LA and upon addition of 18 equivalents of KOTf, showing that only for **1** the added LA impacts the CV response. Cyclic voltammograms were collected at 100 mV/s in 0.25 M TBAPF<sub>6</sub> in MeCN containing 0.5 mM of complex **1** under Ar.

## XI. Impact of $\text{Ca}(\text{OTf})_2$ on the Ligand-Centered Redox Couple

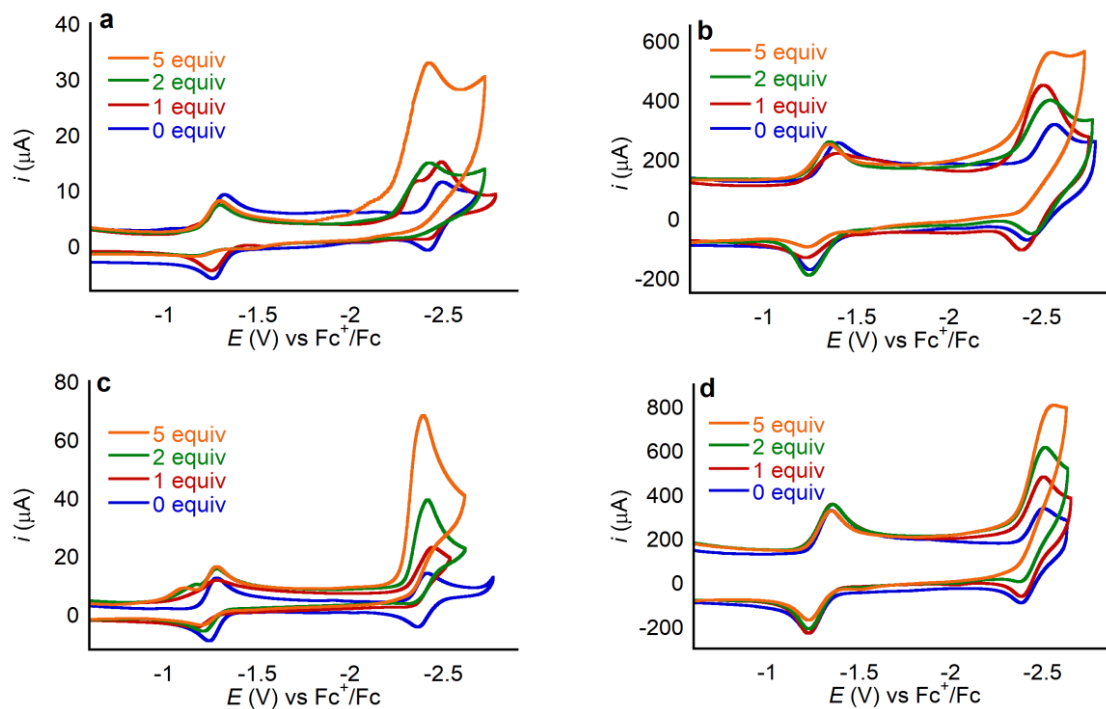


**Figure S43.** Cyclic voltammograms collected for 0.5 mM of cobalt-porphyrin complex at increasing molar equivalents of  $\text{Ca}(\text{OTf})_2$  in 0.25 M TBAPF<sub>6</sub> in MeCN showing the Co(II)/Co(I) couple and the more negative ligand-based redox event near -2.5 V vs  $\text{Fc}^+/\text{Fc}$ . (a) Complex 1 at 100 mV/s, (b) complex 1 at 25 V/s, (c) complex 2 at 100 mV/s, and (d) complex 2 at 25 V/s.

## XI. Cyclic Voltammograms with Trivalent Cations

Adding one equivalent of a trivalent cation triflate salt caused only small changes in the CV response of **1**, with shifts in the Co(II)/Co(I) couple of just 4 and 13 mV for Al(OTf)<sub>3</sub> and Y(OTf)<sub>3</sub> respectively. We hypothesize that the small and highly acidic Al(III) and Y(III) cations have strong ion-pairing to the OTf<sup>-</sup> and PF<sub>6</sub><sup>-</sup> anions present in the solution hindering their ability to bind to the 12-O<sub>3</sub>N aza-crown ether group of **1**. Adding higher amounts of the trivalent ion salts leads to a loss of reversibility of the Co(II)/Co(I) couple of **1** and a discoloration of the solution going from a deep red characteristic of **1** to a greenish brown color. We interpret these changes as indicative of decomposition of **1** in presence of an excess of Al(OTf)<sub>3</sub> and Y(OTf)<sub>3</sub>.

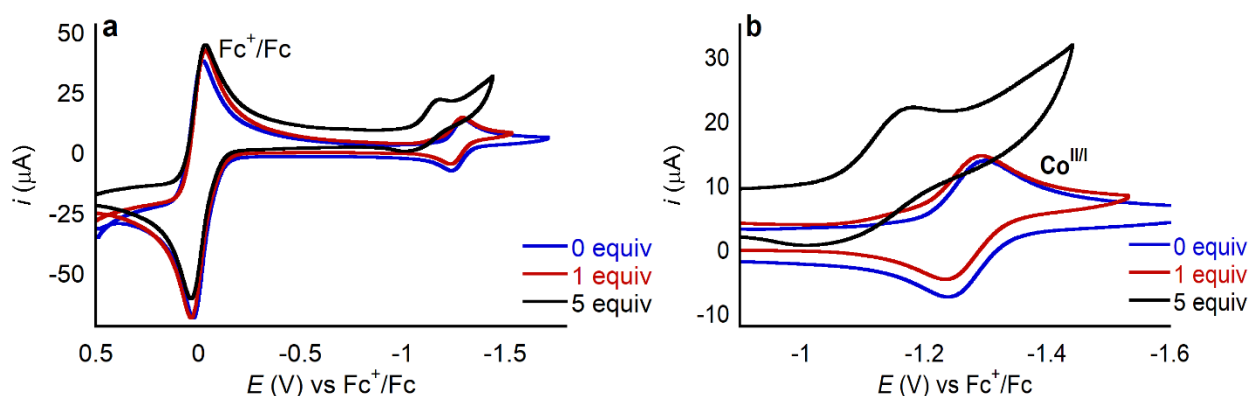


**Figure S44.** (a) Cyclic voltammograms of **1** with increasing amounts of Al(OTf)<sub>3</sub>, (b) Co(II)/Co(I) region of the CV. Cyclic voltammograms were collected at 100 mV/s in 0.25 M TBAPF<sub>6</sub> in MeCN containing 0.5 mM of complex **1** and 1 mM ferrocene under Ar.

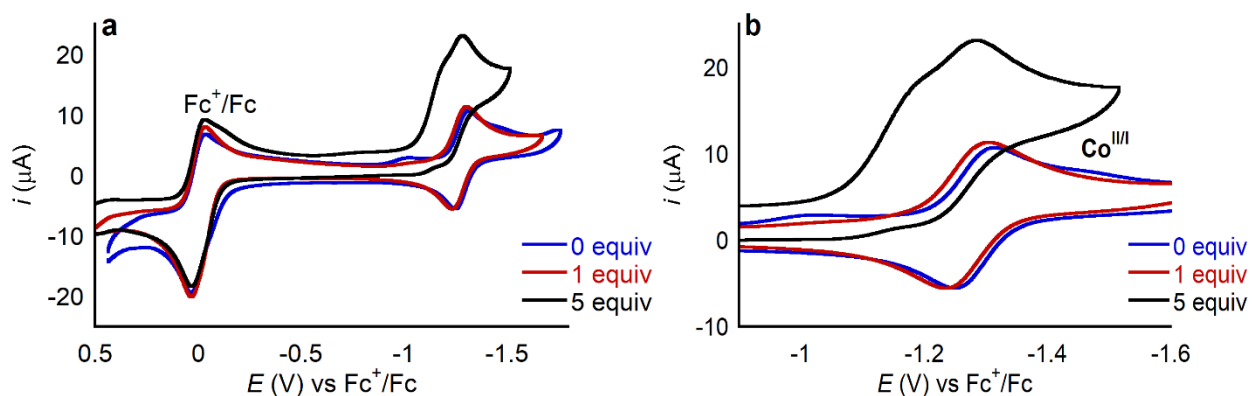


**Figure S45.** (a) Cyclic voltammograms of **1** with increasing amounts of Y(OTf)<sub>3</sub>, (b) Co(II)/Co(I) region of the CV. Cyclic voltammograms were collected at 100 mV/s in 0.25 M TBAPF<sub>6</sub> in MeCN containing 0.5 mM of complex **1** and 0.5 mM ferrocene under Ar.

## XII. Cyclic Voltammograms at Varying Ionic Strengths

**Table S4.** Summary of potential shift ( $\Delta E_{1/2}$ ) seen for the Co(II)/Co(I) couple of **1** upon addition of one equivalent of Ca(OTf)<sub>2</sub> at different ionic strengths (*I*). Cyclic voltammograms were collected at each ionic strength with and without Ca(OTf)<sub>2</sub>,  $E_{1/2}$  values for both cases are also shown here. Cyclic voltammograms were collected using 0.5 mM **1** in MeCN at 100 mV/s under Ar. The concentration of TBAPF<sub>6</sub> in each experiment equals *I*.

<i>I</i> (M)	$\Delta E_{1/2}$ Co(II/I) (mV)	$E_{1/2}$ Co(II/I) (V) vs Fc <sup>+</sup> /Fc	
		<b>1</b> (no added Ca <sup>2+</sup> )	<b>1</b> (1 equiv Ca <sup>2+</sup> )
0.5	48	-1.305	-1.257
0.1	43	-1.298	-1.255
0.25	34	-1.282	-1.248
0.5	29	-1.270	-1.241
0.75	25	-1.265	-1.240
1.0	16	-1.260	-1.245

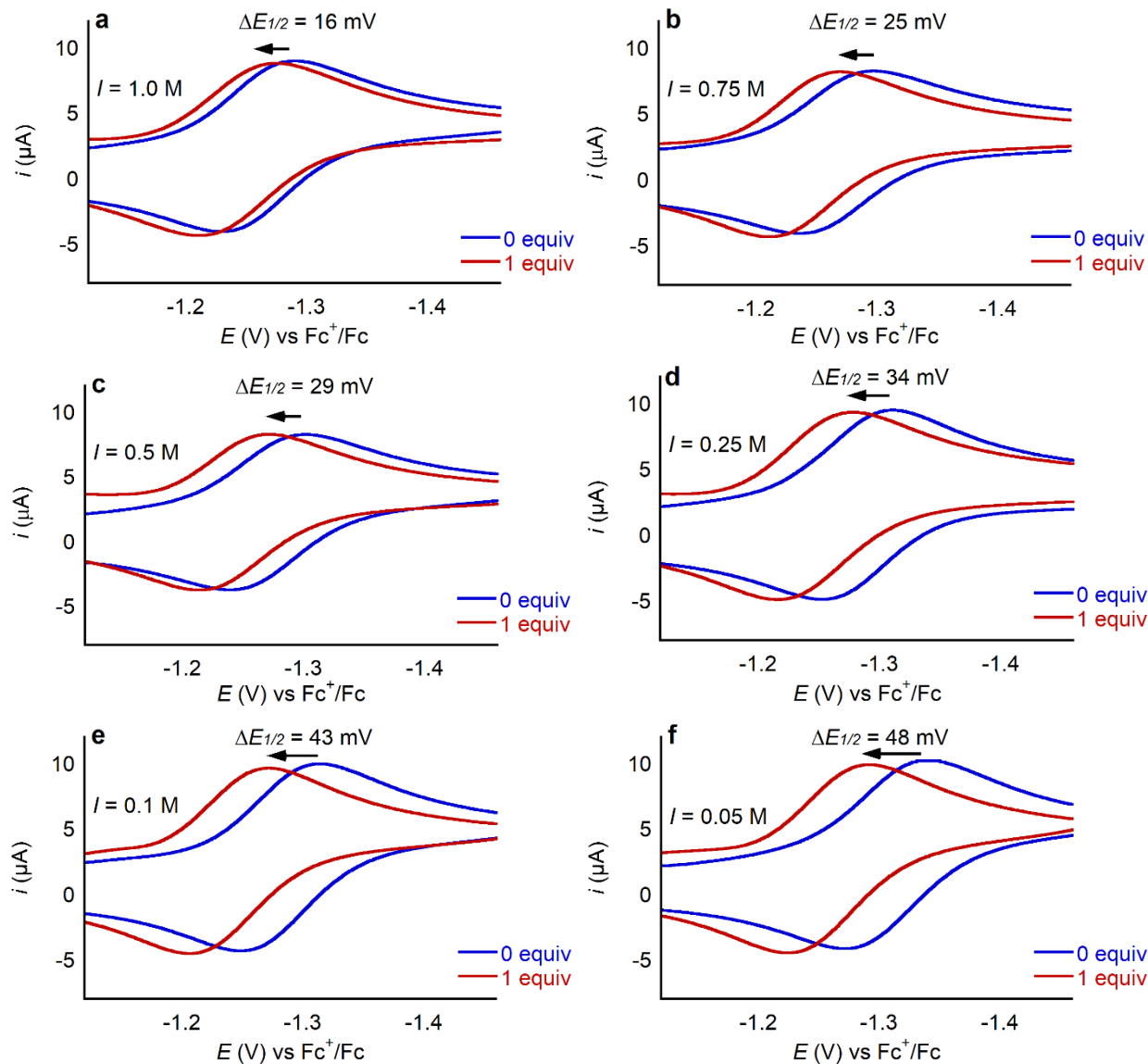


**Figure S46.** Cyclic voltammograms of the Co(II)/Co(I) couple of **1** in absence of LA and upon addition of 1 equivalent of  $\text{Ca}(\text{OTf})_2$ , at different ionic strengths ( $I$ ). Cyclic voltammograms were collected under Ar at 100 mV/s in MeCN containing 1 mM ferrocene and 0.5 mM of **1**. The molar concentration of  $\text{TBAPF}_6$  electrolyte is equal to the ionic strength.

### XIII. Computational Results

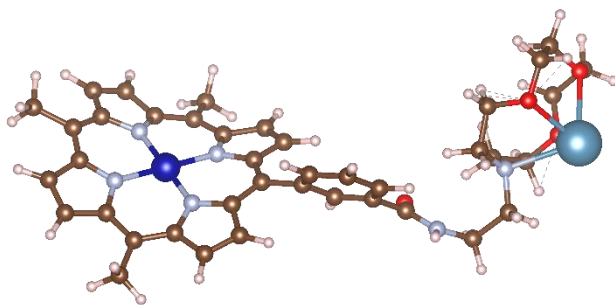


**Figure S47.** Optimized geometry of  $1^*-\text{Ca}^{2+}$  with an extended arm between the porphyrin and aza-crown ether.

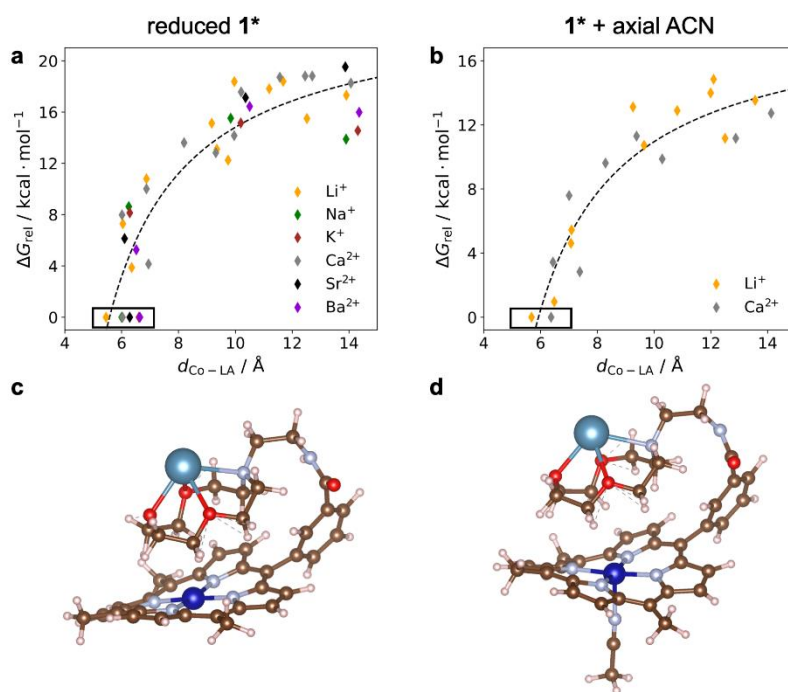


**Figure S48.** DFT calculated relative free energies of various conformers sampled for (a) reduced  $1^*$  (i.e., a Co(I) center) and (b)  $1^*$  (i.e., a Co(II) center) with an explicit axial acetonitrile ligand as functions of the Co–LA distance. The most stable conformers are indicated by the black box, and the black dashed line is used to guide the eye. Optimized geometries of (c) reduced  $1^*-\text{Ca}^{2+}$  and (d)  $1^*-\text{Ca}^{2+}$  with an explicit axial acetonitrile ligand.

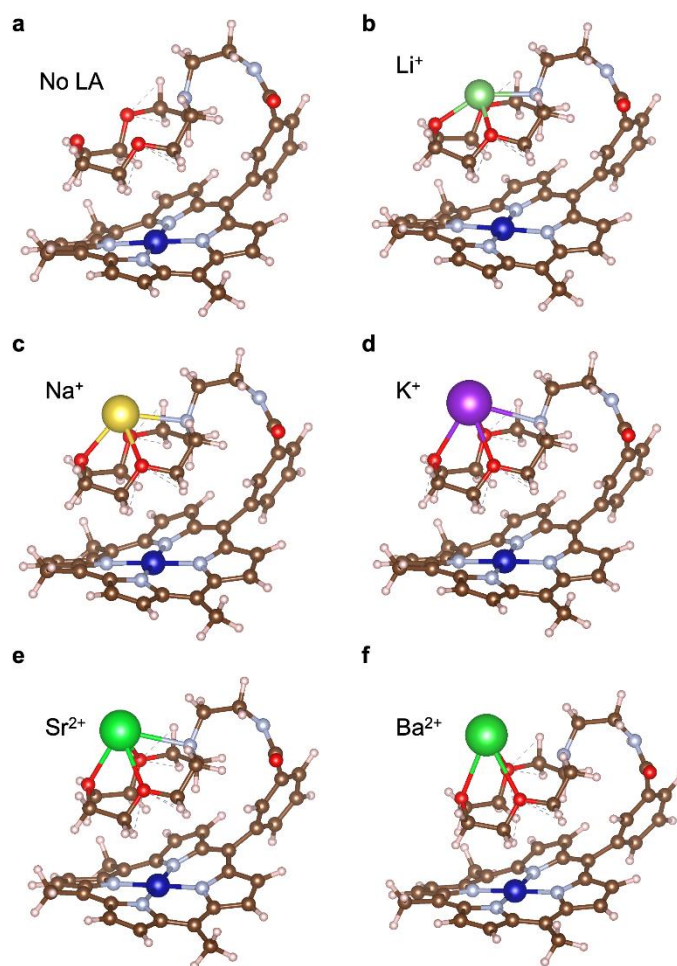


**Figure S49.** Optimized geometries of **1\***-LA without an axial acetonitrile ligand.

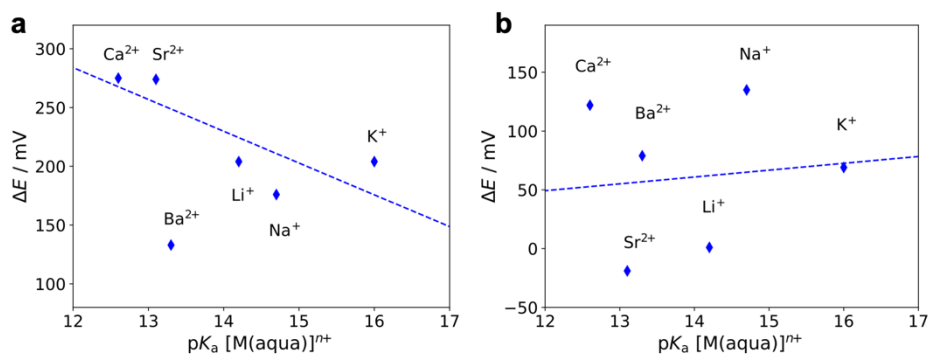


**Figure S50.** Calculated relative reduction potentials of the Co(II)/Co(I) couple of **1\*** when LAs are bound to the aza-crown ether as a function of the LA strength. These calculations were performed for the most stable geometry. An axial acetonitrile ligand was not included in these calculations. The data for Ba<sup>2+</sup> is excluded in the linear fit.

#### XIV. Including Ionic Strength and Counterion Effects in the Computational Model

We explored the possibility that the disparity between the calculated and experimental reduction potentials is due to the presence of electrolyte in the experiments. We focused on two possible reasons: screening of the cationic LA from the Co center and counterion interactions between the cationic LA and anions, which reduce the electrostatic field of the LA. For the screening effect, we calculated the relative reduction potential of the  $\text{Co}^{\text{II}}/\text{Co}^{\text{I}}$  couple for  $\mathbf{1}^*\text{-Li}^+$  and  $\mathbf{1}^*\text{-Ca}^{2+}$  with ionic strength  $I = 0$  M or 0.25 M using the integral equation formalism variant of the polarizable continuum model (IEF-PCM). Given this solvent model is different from the C-PCM solvent model used in the main text, a new reference calculation at  $I = 0$  M was necessary. In the IEF-PCM approach, the ions of the electrolyte are modeled implicitly, and the ionic strength is a parameter used to calculate the Debye screening length in the Poisson-Boltzmann equation. Due to the limitations of the software used for these calculations, geometry optimizations and frequency analyses could not be performed. We therefore only calculated  $\Delta E$  based on the relative energies with the same geometry as that used for Figure 11 for both the  $I = 0$  M and 0.25 M, assuming that there is no significant structural change and that the zero-point energy and entropic terms cancel. For the counterion effect, we added an explicit  $\text{Cl}^-$  ion near the LA and calculated the reduction potentials using the same procedure (geometry optimization followed by frequency calculations) as described in the Methods section.

As shown in Table S5, for both models, we observed a decrease in the reduction potential of  $\mathbf{1}^*\text{-Li}$  and  $\mathbf{1}^*\text{-Ca}$  relative to  $\mathbf{1}^*$  with no LA bound, leading to better agreement with the experimental results. In contrast, for both models we observed only small changes,  $\leq 44$  mV, in the difference of relative reduction potential ( $\Delta\Delta E = \Delta E(\text{Ca}^{2+}) - \Delta E(\text{Li}^+)$ ), suggesting that the calculated trend of reduction potential vs. LA strength is not significantly affected. These results indicate that the overestimation of the relative reduction potentials could be partially due to the absence of electrolyte in the model. However, due to the simplification in the models, quantitative agreement was not achieved and regardless of the specific model there is still a significant difference between calculated and experimental data. To fully understand the influence of the electrolyte, an explicit solvent model with electrolyte ions is necessary but is beyond the scope of this work.

Table S5. Calculated Relative Reduction Potential of the  $\text{Co}^{\text{II}}/\text{Co}^{\text{I}}$  couple for  $\mathbf{1}^*\text{-Li}^+$  and  $\mathbf{1}^*\text{-Ca}^{2+}$  with Different Ionic Strength or Explicit Anion

	Method	$\Delta E(\text{Ca}^{2+}) / \text{mV}^{\text{a}}$	$\Delta E(\text{Li}^+) / \text{mV}^{\text{a}}$	$\Delta\Delta E = \Delta E(\text{Ca}^{2+}) - \Delta E(\text{Li}^+) / \text{mV}$
Ionic strength	0 M	321	180	141
	0.25 M	279	129	150
Counterion effect	w/o explicit anion	261	143	118
	w/ one $\text{Cl}^-$ ion	159 <sup>b</sup>	-3 <sup>b</sup>	162

<sup>a</sup>For each model, the reduction potential of  $\mathbf{1}^*$  with no LA bound was used as reference to calculate the relative reduction potential  $\Delta E$ . The ionic strength calculations were performed with the IEF-PCM solvent model and compare energies for geometries optimized with the C-PCM solvent model. The counterion effect calculations were performed with the C-PCM solvent model and compare free energies for fully optimized geometries with this solvent model. Thus, the results for the counterion effect without an explicit anion are the same as those presented in Figure 11.

<sup>b</sup>The  $\text{Cl}^-$  anion is not included in the calculation of the reference system ( $\mathbf{1}^*$  with no LA bound), because a  $\text{Cl}^-$  anion is unlikely to bind to the aza-crown ether without a cation present.

## Optimized Structures

The optimized structures of the most stable conformer for **1\***-LA with Co(II) center are listed below.

**1\* no LA** (E(UB-P86) = -63247.85394861 eV)

93

0 2

N	-3.026653	1.732676	-0.338558
N	-3.052989	-0.771710	0.834666
N	-0.564402	-0.275578	1.945840
N	-0.604395	2.269124	0.854076
C	-3.020465	3.100642	-0.592153
C	-4.054394	3.433090	-1.546241
C	-4.656931	2.258126	-1.912362
C	-4.050770	1.208767	-1.123892
C	-4.540488	-0.103332	-1.048761
C	-4.114051	-0.982852	-0.039440
C	-4.768367	-2.234043	0.265555
C	-4.127172	-2.767180	1.354442
C	-3.034447	-1.877059	1.680655
C	-2.006340	-2.202388	2.580222
C	-0.805432	-1.477938	2.606099
C	0.423764	-1.986912	3.172745
C	1.422563	-1.120667	2.811767
C	0.793682	-0.022952	2.110029
C	1.439071	1.171341	1.740053
C	0.727611	2.273400	1.235871
C	1.276128	3.606540	1.141251
C	0.254582	4.428870	0.739500
C	-0.902286	3.588952	0.520505
C	-2.082074	4.023844	-0.101135
H	-4.264109	4.431862	-1.922253
H	-5.474415	2.123937	-2.616938
H	-5.626278	-2.637246	-0.268218
H	-4.344188	-3.707919	1.855078
H	0.526358	-2.923317	3.716856
H	2.487205	-1.205917	3.014252
H	2.304493	3.867596	1.382647
H	0.291985	5.502180	0.564589
C	2.926020	1.224478	1.755367
C	3.543603	1.419377	0.507596
C	3.740038	0.920761	2.868084
C	4.904791	1.133704	0.318892
H	2.926435	1.663539	-0.361063
C	5.120316	0.722104	2.699738
H	3.284527	0.814329	3.855771
C	5.700787	0.769026	1.420101
H	5.741961	0.489925	3.568162
H	6.758522	0.529520	1.281674
C	5.268596	0.982263	-1.132613
O	4.993623	1.851230	-1.979817

N	5.713481	-0.279317	-1.467136
H	5.781864	-0.941547	-0.693251
C	5.318341	-0.853275	-2.754287
H	5.072229	0.000134	-3.404898
H	6.156940	-1.403752	-3.212923
Co	-1.811954	0.736820	0.824820
C	-5.632059	-0.563808	-1.993378
H	-5.657176	0.036697	-2.911465
H	-5.470933	-1.611398	-2.290174
H	-6.628638	-0.502846	-1.523257
C	-2.104624	-3.485356	3.378746
H	-1.537725	-3.418959	4.317357
H	-3.145895	-3.720132	3.639214
H	-1.700299	-4.334868	2.800474
C	-2.268233	5.501340	-0.380765
H	-1.883677	6.110348	0.449955
H	-1.736032	5.813888	-1.295049
H	-3.329729	5.753187	-0.508412
C	4.097226	-1.818654	-2.618128
H	4.430744	-2.730812	-2.094133
H	3.836764	-2.125223	-3.650624
C	2.803031	-1.596326	-0.506018
C	2.334169	-0.096361	-2.483612
C	2.440889	-3.058567	-0.181097
H	2.026894	-0.944686	-0.079268
H	3.723438	-1.351337	0.069671
H	2.334853	-0.207276	-3.584759
H	2.931676	0.818396	-2.274128
C	0.891371	0.177122	-2.054880
H	3.230334	-3.738636	-0.546832
H	2.393089	-3.152595	0.926538
H	0.790940	0.291449	-0.949181
H	0.570590	1.146728	-2.492737
C	0.065520	-3.026257	-0.124575
H	0.049039	-1.920279	-0.099975
H	0.039560	-3.365478	0.934197
C	-1.266843	-0.821413	-2.086797
H	-1.321294	-0.744519	-0.973604
H	-1.800813	0.068250	-2.484492
C	-1.174639	-3.589387	-0.818069
H	-1.135760	-4.690259	-0.746227
H	-2.074481	-3.239930	-0.272726
C	-1.966747	-2.101360	-2.547852
H	-2.996436	-2.107650	-2.134596
H	-2.031713	-2.101904	-3.648032
O	0.080428	-0.893949	-2.519364
O	-1.267669	-3.300723	-2.217857
O	1.230708	-3.518941	-0.783131
N	2.906499	-1.328699	-1.939311

1\*-Li<sup>+</sup> (E(UB-P86) = -63452.10303429 eV)

94

1 2

N	-2.952631	1.751850	-0.412988
N	-2.990405	-0.683842	0.892355
N	-0.543591	-0.109832	2.033410
N	-0.554726	2.351178	0.778386
C	-2.954386	3.106252	-0.730086
C	-3.978158	3.383201	-1.713486
C	-4.559769	2.184999	-2.036446
C	-3.955739	1.179687	-1.190311
C	-4.435974	-0.132757	-1.060062
C	-4.032370	-0.951327	0.009364
C	-4.704572	-2.171523	0.391682
C	-4.103739	-2.617275	1.542669
C	-3.011567	-1.713704	1.829473
C	-2.017835	-1.967750	2.789014
C	-0.808139	-1.254422	2.781561
C	0.409963	-1.737547	3.390933
C	1.426559	-0.921160	2.962987
C	0.819274	0.131387	2.179037
C	1.478679	1.290706	1.728743
C	0.775903	2.368762	1.162876
C	1.331428	3.692365	0.995150
C	0.314041	4.495971	0.547224
C	-0.845790	3.650763	0.371777
C	-2.022830	4.055219	-0.275829
H	-4.193267	4.360723	-2.139604
H	-5.363650	2.006950	-2.746855
H	-5.552506	-2.609861	-0.130387
H	-4.349424	-3.508511	2.115271
H	0.494670	-2.628868	4.007955
H	2.487734	-1.007940	3.182192
H	2.360033	3.962135	1.225280
H	0.355888	5.557955	0.315350
C	2.966015	1.329637	1.714124
C	3.549460	1.445497	0.440193
C	3.809815	1.090197	2.820043
C	4.902723	1.137722	0.230130
H	2.904317	1.636593	-0.421827
C	5.184457	0.875928	2.624270
H	3.384994	1.049873	3.825878
C	5.728868	0.839191	1.328324
H	5.829824	0.695748	3.487274
H	6.780101	0.581367	1.175306
C	5.202416	0.862954	-1.218580
O	4.908030	1.661563	-2.125720
N	5.578667	-0.439990	-1.458977
H	5.721719	-1.028924	-0.638737
C	5.165137	-1.106676	-2.692554
H	4.931242	-0.301889	-3.405945

H	5.992826	-1.702706	-3.110713
Co	-1.764315	0.832676	0.832105
C	-5.504541	-0.641845	-2.005861
H	-5.480592	-0.110935	-2.966805
H	-5.360973	-1.711747	-2.220829
H	-6.514913	-0.523663	-1.579785
C	-2.165851	-3.158344	3.713854
H	-1.618231	-3.005161	4.654139
H	-3.219233	-3.337220	3.971811
H	-1.777662	-4.078348	3.242167
C	-2.208982	5.518200	-0.620913
H	-1.850171	6.162849	0.194878
H	-1.652817	5.796805	-1.531875
H	-3.268006	5.757283	-0.786798
C	3.942837	-2.054156	-2.506738
H	4.246054	-2.923083	-1.899407
H	3.701777	-2.441473	-3.513653
C	2.659662	-1.553802	-0.429890
C	2.250343	-0.247025	-2.532673
C	2.310986	-2.954693	0.080630
H	1.887128	-0.853796	-0.076572
H	3.598187	-1.228800	0.055731
H	2.302937	-0.399308	-3.626047
H	2.893937	0.626628	-2.310713
C	0.808123	0.093159	-2.165621
H	3.088279	-3.683860	-0.199664
H	2.227193	-2.934229	1.182788
H	0.686511	0.333216	-1.085507
H	0.476659	0.982763	-2.732298
C	-0.112003	-2.997566	0.152101
H	-0.171496	-1.890667	0.158455
H	-0.124068	-3.335959	1.204779
C	-1.371576	-0.954016	-2.152304
H	-1.477083	-0.766678	-1.062961
H	-1.875298	-0.124919	-2.683522
C	-1.278961	-3.631647	-0.597394
H	-1.229225	-4.725026	-0.473283
H	-2.238674	-3.271595	-0.185434
C	-1.995409	-2.298218	-2.514259
H	-3.028288	-2.351549	-2.124757
H	-2.017526	-2.425832	-3.607250
O	0.012311	-1.050488	-2.508586
O	-1.203785	-3.399381	-2.024436
O	1.088741	-3.451836	-0.505185
N	2.702984	-1.512335	-1.910668
Li	0.904053	-2.885579	-2.467658

1\*-Na<sup>+</sup> (E(UB-P86) = -63253.15347352 eV)

94

1 2

N	-3.020744	1.740266	-0.520598
N	-3.091477	-0.595325	0.967299
N	-0.635958	0.031746	2.071308
N	-0.624752	2.412902	0.650180
C	-2.999896	3.064280	-0.946770
C	-4.023134	3.280683	-1.945338
C	-4.633002	2.073579	-2.163851
C	-4.039830	1.127273	-1.245376
C	-4.537987	-0.163720	-1.016100
C	-4.137138	-0.910124	0.105246
C	-4.816063	-2.100433	0.560872
C	-4.212445	-2.484240	1.731356
C	-3.112733	-1.572804	1.960105
C	-2.111605	-1.784652	2.921869
C	-0.901505	-1.074883	2.874223
C	0.314356	-1.526528	3.512280
C	1.331419	-0.730183	3.051327
C	0.725033	0.284521	2.217591
C	1.385284	1.424290	1.723204
C	0.694179	2.460343	1.070850
C	1.256281	3.768741	0.823853
C	0.256703	4.534271	0.281270
C	-0.899402	3.678240	0.135095
C	-2.059342	4.036354	-0.567002
H	-4.222911	4.225423	-2.446527
H	-5.447248	1.857696	-2.851664
H	-5.669773	-2.562816	0.070021
H	-4.461316	-3.339201	2.355257
H	0.397909	-2.388512	4.169872
H	2.392264	-0.807487	3.275175
H	2.276946	4.057228	1.065355
H	0.309258	5.575090	-0.029473
C	2.871247	1.484952	1.760022
C	3.503203	1.567494	0.507500
C	3.676534	1.309592	2.906330
C	4.872793	1.299744	0.363209
H	2.890906	1.706929	-0.386965
C	5.063725	1.131694	2.773794
H	3.213442	1.290487	3.895911
C	5.663469	1.071175	1.503538
H	5.677265	1.002614	3.668480
H	6.728944	0.848224	1.403203
C	5.239144	0.993954	-1.062759
O	4.950338	1.753577	-2.004941
N	5.677463	-0.298551	-1.248153
H	5.795812	-0.858950	-0.404129
C	5.323063	-1.016838	-2.470539
H	5.083857	-0.243677	-3.216345

H	6.181910	-1.597813	-2.845161
Co	-1.844230	0.900132	0.796451
C	-5.618868	-0.730696	-1.914047
H	-5.641586	-0.231220	-2.891164
H	-5.451501	-1.802860	-2.100945
H	-6.618489	-0.628913	-1.458502
C	-2.248730	-2.935406	3.897551
H	-1.717095	-2.730162	4.837399
H	-3.300705	-3.126563	4.151528
H	-1.832302	-3.864859	3.470639
C	-2.220815	5.461136	-1.056483
H	-1.793403	6.178355	-0.341749
H	-1.717282	5.615438	-2.026033
H	-3.280481	5.719296	-1.187076
C	4.123275	-1.996522	-2.289846
H	4.437920	-2.839910	-1.651812
H	3.937847	-2.415868	-3.296961
C	2.750029	-1.504189	-0.273547
C	2.351510	-0.274124	-2.424630
C	2.397144	-2.894399	0.274481
H	1.965819	-0.798824	0.039554
H	3.668982	-1.160935	0.240476
H	2.415568	-0.470976	-3.511025
H	2.966520	0.631960	-2.244599
C	0.900292	0.064387	-2.082350
H	3.179950	-3.625068	0.011465
H	2.330350	-2.831182	1.378414
H	0.770803	0.335297	-1.009553
H	0.587565	0.950610	-2.668250
C	-0.005509	-2.880203	0.333221
H	-0.026882	-1.777873	0.238105
H	-0.029812	-3.111901	1.416102
C	-1.275508	-0.936021	-1.989252
H	-1.326805	-0.717417	-0.898716
H	-1.794530	-0.106998	-2.510105
C	-1.221198	-3.527733	-0.324635
H	-1.188232	-4.612297	-0.131389
H	-2.144032	-3.117842	0.126098
C	-1.972446	-2.265545	-2.269522
H	-2.995392	-2.234887	-1.850676
H	-2.039803	-2.433843	-3.356019
O	0.084588	-1.068774	-2.401123
O	-1.244605	-3.396810	-1.761475
O	1.176597	-3.431877	-0.267946
N	2.851448	-1.487124	-1.746927
Na	1.049778	-3.289132	-2.655519

**1\*-K<sup>+</sup>** (E(UB-P86) = -64013.51031793 eV)

94

1 2

N	-3.098554	1.641932	-0.765466
N	-3.151346	-0.456113	1.039096
N	-0.733406	0.375723	2.082051
N	-0.754480	2.547514	0.362053
C	-3.079609	2.881772	-1.393961
C	-4.049345	2.909811	-2.465232
C	-4.631444	1.670148	-2.514530
C	-4.071174	0.896141	-1.428745
C	-4.554026	-0.355341	-1.017589
C	-4.169173	-0.917722	0.212008
C	-4.836489	-2.041940	0.826110
C	-4.256406	-2.232533	2.054688
C	-3.179766	-1.273167	2.166523
C	-2.198026	-1.316713	3.169623
C	-0.996333	-0.605091	3.034423
C	0.213275	-0.932577	3.754713
C	1.225613	-0.192689	3.199184
C	0.617530	0.679635	2.217547
C	1.257743	1.766453	1.593021
C	0.548657	2.693410	0.807818
C	1.073426	3.981470	0.416605
C	0.068710	4.636357	-0.247917
C	-1.052356	3.725084	-0.322230
C	-2.187651	3.932683	-1.118969
H	-4.236406	3.757318	-3.120782
H	-5.403458	1.331041	-3.201425
H	-5.665907	-2.592879	0.388254
H	-4.504227	-2.988500	2.796327
H	0.296949	-1.689116	4.532427
H	2.283232	-0.215314	3.447814
H	2.076033	4.332401	0.650813
H	0.101402	5.632066	-0.685482
C	2.740052	1.874867	1.653967
C	3.406364	1.839738	0.416244
C	3.516356	1.829898	2.832965
C	4.782364	1.576418	0.338216
H	2.822310	1.878671	-0.506740
C	4.907300	1.649914	2.758068
H	3.026757	1.913979	3.806509
C	5.541237	1.464119	1.517461
H	5.495319	1.617586	3.678171
H	6.610297	1.241665	1.467695
C	5.196851	1.133556	-1.036714
O	4.894631	1.772923	-2.060612
N	5.714671	-0.143467	-1.074729
H	5.825628	-0.607769	-0.172968
C	5.396815	-1.011665	-2.206980
H	5.124599	-0.342815	-3.037832

H	6.280827	-1.594461	-2.515021
Co	-1.937838	1.033518	0.684229
C	-5.597020	-1.078443	-1.845197
H	-5.595263	-0.739762	-2.888731
H	-5.409881	-2.163334	-1.849000
H	-6.611205	-0.923010	-1.440668
C	-2.355785	-2.284907	4.324252
H	-1.827632	-1.927755	5.219213
H	-3.412567	-2.415842	4.594390
H	-1.951756	-3.279695	4.070178
C	-2.364703	5.260367	-1.827646
H	-1.960942	6.087385	-1.227784
H	-1.844404	5.271515	-2.800867
H	-3.425855	5.477920	-2.014007
C	4.241400	-2.011496	-1.895864
H	4.596536	-2.747626	-1.153787
H	4.084709	-2.570437	-2.839637
C	2.825414	-1.355007	0.043666
C	2.380992	-0.415742	-2.243183
C	2.515834	-2.684078	0.752006
H	2.017528	-0.642496	0.266036
H	3.722300	-0.923056	0.532440
H	2.464494	-0.741220	-3.295918
H	2.936437	0.544406	-2.184221
C	0.908503	-0.118667	-1.952342
H	3.329655	-3.408979	0.579727
H	2.453117	-2.485415	1.842311
H	0.753623	0.275929	-0.921055
H	0.564797	0.678068	-2.642446
C	0.123403	-2.711292	0.771900
H	0.084573	-1.646516	0.478748
H	0.090449	-2.740116	1.879591
C	-1.219026	-1.176742	-1.761484
H	-1.294024	-0.809861	-0.712008
H	-1.758843	-0.444411	-2.395716
C	-1.088745	-3.477462	0.245642
H	-1.036699	-4.514905	0.614973
H	-2.007923	-3.007712	0.647073
C	-1.883467	-2.549881	-1.854568
H	-2.910922	-2.473693	-1.450098
H	-1.943602	-2.869039	-2.907057
O	0.148469	-1.314972	-2.137429
O	-1.151527	-3.587960	-1.188296
O	1.321338	-3.337394	0.294041
N	2.952461	-1.493973	-1.417606
K	1.345743	-3.892286	-2.457055

1\*-Ca<sup>2+</sup> (E(UB-P86) = -64240.63677155 eV)

94

2 2

N	-3.018166	1.655494	-0.780823
N	-3.054509	-0.356900	1.121948
N	-0.640206	0.538932	2.118496
N	-0.669742	2.609324	0.273030
C	-3.011326	2.865747	-1.465855
C	-3.995139	2.842412	-2.524791
C	-4.569641	1.598298	-2.513461
C	-3.994964	0.878442	-1.398533
C	-4.481492	-0.347384	-0.920515
C	-4.092451	-0.846386	0.334949
C	-4.772017	-1.920103	1.021933
C	-4.174562	-2.054548	2.250002
C	-3.081422	-1.108984	2.296339
C	-2.089844	-1.107512	3.291116
C	-0.890384	-0.398781	3.116041
C	0.330143	-0.697868	3.831186
C	1.334698	0.022500	3.234153
C	0.713958	0.841908	2.216975
C	1.352368	1.878294	1.512935
C	0.643259	2.763519	0.683742
C	1.176560	4.020107	0.209671
C	0.163749	4.651740	-0.465249
C	-0.968979	3.751284	-0.466253
C	-2.118721	3.929516	-1.249329
H	-4.195936	3.659883	-3.213585
H	-5.348829	1.222047	-3.172237
H	-5.619743	-2.477906	0.630164
H	-4.426224	-2.765651	3.033220
H	0.424414	-1.414937	4.643764
H	2.394069	0.024790	3.478745
H	2.187688	4.370069	0.405961
H	0.195097	5.621658	-0.957681
C	2.837317	1.962322	1.527481
C	3.459992	1.758259	0.284796
C	3.648322	2.065956	2.677791
C	4.830856	1.471537	0.198890
H	2.840961	1.687623	-0.614045
C	5.036920	1.874304	2.580288
H	3.187598	2.270901	3.646979
C	5.629398	1.520032	1.355318
H	5.656681	1.962691	3.475340
H	6.695776	1.287123	1.301502
C	5.194457	0.863868	-1.126636
O	4.923816	1.411153	-2.210710
N	5.608629	-0.445159	-1.031306
H	5.724273	-0.826702	-0.092523
C	5.300785	-1.386913	-2.102559
H	5.089463	-0.775684	-2.993202

H	6.173559	-2.022442	-2.327348
Co	-1.850245	1.119746	0.691778
C	-5.536530	-1.094210	-1.711931
H	-5.435964	-0.904383	-2.789322
H	-5.448046	-2.180933	-1.564287
H	-6.556228	-0.799283	-1.412023
C	-2.217344	-2.051899	4.468648
H	-1.684007	-1.670217	5.350121
H	-3.266989	-2.199749	4.755935
H	-1.795290	-3.041960	4.222683
C	-2.307565	5.229213	-2.004025
H	-1.900719	6.077944	-1.436862
H	-1.796284	5.207458	-2.981904
H	-3.371302	5.436403	-2.187053
C	4.112369	-2.336506	-1.785386
H	4.394301	-3.025834	-0.972445
H	3.996620	-2.951928	-2.696052
C	2.644622	-1.405926	0.009903
C	2.343860	-0.694862	-2.361380
C	2.245802	-2.603876	0.872188
H	1.864271	-0.636518	0.113458
H	3.559846	-0.954022	0.427358
H	2.452737	-1.101789	-3.381491
H	2.976340	0.212991	-2.315243
C	0.887565	-0.280525	-2.149392
H	3.011749	-3.396443	0.842112
H	2.112923	-2.274288	1.918411
H	0.727682	0.253270	-1.185239
H	0.588216	0.414752	-2.954659
C	-0.184148	-2.592469	0.844481
H	-0.218946	-1.534684	0.523362
H	-0.229716	-2.610220	1.948112
C	-1.316700	-1.220458	-1.925796
H	-1.434749	-0.733420	-0.936089
H	-1.760311	-0.545467	-2.681254
C	-1.352077	-3.398206	0.287298
H	-1.305496	-4.422907	0.687331
H	-2.308507	-2.939763	0.586510
C	-2.016012	-2.576775	-1.931745
H	-3.047818	-2.474840	-1.556719
H	-2.041999	-2.992188	-2.950708
O	0.075491	-1.466846	-2.183233
O	-1.290217	-3.554825	-1.154064
O	1.030639	-3.229771	0.394975
N	2.779687	-1.771199	-1.429584
Ca	1.082184	-3.857506	-1.999745

1\*-Sr<sup>2+</sup> (E(UB-P86) = -64074.51431556 eV)

94

2 2

N	-3.308137	1.411110	-0.979708
N	-3.160443	-0.393071	1.107290
N	-0.879532	0.849706	2.023070
N	-1.092815	2.709946	-0.011625
C	-3.436287	2.554500	-1.759755
C	-4.393336	2.326715	-2.819071
C	-4.814075	1.026988	-2.709935
C	-4.174406	0.472536	-1.536138
C	-4.513303	-0.758037	-0.953968
C	-4.099196	-1.084781	0.350250
C	-4.653221	-2.172692	1.121358
C	-4.085144	-2.111602	2.369824
C	-3.128070	-1.027589	2.347265
C	-2.180663	-0.796443	3.359000
C	-1.062091	0.019490	3.125750
C	0.159643	-0.056120	3.894750
C	1.104527	0.679889	3.224538
C	0.432720	1.304572	2.105701
C	0.973894	2.328834	1.306823
C	0.190289	3.045175	0.385921
C	0.585254	4.306229	-0.200107
C	-0.488356	4.762628	-0.921453
C	-1.513763	3.744975	-0.842988
C	-2.674912	3.728987	-1.629314
H	-4.676096	3.056261	-3.574948
H	-5.531408	0.508437	-3.342159
H	-5.404706	-2.873372	0.764053
H	-4.267359	-2.773176	3.213237
H	0.299811	-0.653410	4.792511
H	2.152787	0.812590	3.480140
H	1.548111	4.787042	-0.040270
H	-0.562231	5.683036	-1.496466
C	2.436362	2.595341	1.353482
C	3.132520	2.364588	0.155096
C	3.179734	2.896391	2.515653
C	4.530855	2.247003	0.140405
H	2.569175	2.141760	-0.755127
C	4.583987	2.872352	2.481986
H	2.656370	3.131316	3.446029
C	5.266378	2.489080	1.314303
H	5.149018	3.113830	3.385663
H	6.353847	2.380867	1.314716
C	5.026415	1.564978	-1.102765
O	4.702468	1.939140	-2.244350
N	5.641181	0.357937	-0.856713
H	5.791592	0.110182	0.121084
C	5.484900	-0.743282	-1.801062
H	5.200919	-0.286875	-2.761087

H	6.442829	-1.269336	-1.947193
Co	-2.115330	1.152376	0.541110
C	-5.427643	-1.724655	-1.678016
H	-5.527259	-1.475034	-2.741501
H	-5.032782	-2.751682	-1.617605
H	-6.437823	-1.737236	-1.235835
C	-2.254946	-1.589059	4.647318
H	-1.809751	-1.031300	5.483032
H	-3.294757	-1.816070	4.920357
H	-1.714652	-2.547695	4.556270
C	-3.020308	4.940056	-2.471864
H	-2.724799	5.870253	-1.966185
H	-2.508354	4.915975	-3.449505
H	-4.101576	4.996527	-2.661741
C	4.434246	-1.802096	-1.360761
H	4.807823	-2.346737	-0.478087
H	4.411829	-2.529118	-2.192688
C	2.843362	-0.916449	0.342406
C	2.453168	-0.503402	-2.093330
C	2.605859	-2.074195	1.317273
H	1.967309	-0.251677	0.379178
H	3.684542	-0.307906	0.719903
H	2.609196	-1.007522	-3.064420
H	2.953965	0.482072	-2.176815
C	0.956254	-0.253942	-1.901763
H	3.469280	-2.757923	1.341762
H	2.449943	-1.665431	2.332892
H	0.738086	0.368922	-1.004505
H	0.569402	0.301018	-2.777031
C	0.207555	-2.356378	1.343099
H	0.055567	-1.347449	0.917863
H	0.172628	-2.259557	2.443927
C	-1.108598	-1.401029	-1.496069
H	-1.254221	-0.842602	-0.546577
H	-1.647942	-0.850026	-2.289714
C	-0.880159	-3.333057	0.908750
H	-0.717525	-4.296346	1.417641
H	-1.872090	-2.942514	1.196380
C	-1.664908	-2.814480	-1.353385
H	-2.697523	-2.774618	-0.967306
H	-1.667161	-3.324623	-2.329668
O	0.292010	-1.521365	-1.779954
O	-0.840947	-3.641043	-0.505163
O	1.480205	-2.896783	0.936183
N	3.040096	-1.388858	-1.054950
Sr	1.622903	-3.932476	-1.503702

**1\*-Ba<sup>2+</sup>** (E(UB-P86) = -63933.71255409 eV)

94

2 2

N	3.423070	-1.112915	-1.254818
N	3.410211	-0.023432	1.295986
N	1.049749	-1.381247	1.871162
N	1.139017	-2.570508	-0.645676
C	3.419914	-1.919829	-2.388608
C	4.397266	-1.447652	-3.341417
C	4.974248	-0.328117	-2.803708
C	4.396347	-0.143410	-1.492204
C	4.856304	0.800442	-0.561627
C	4.429203	0.773164	0.775602
C	5.038202	1.555392	1.824960
C	4.423418	1.203181	2.997425
C	3.388010	0.252455	2.663579
C	2.398209	-0.156297	3.570248
C	1.248463	-0.829749	3.135672
C	0.035523	-0.917967	3.914984
C	-0.915437	-1.496945	3.116201
C	-0.260914	-1.852884	1.876306
C	-0.833293	-2.651233	0.870362
C	-0.112526	-3.039507	-0.271263
C	-0.581194	-4.037796	-1.203334
C	0.400065	-4.193155	-2.145433
C	1.455204	-3.259780	-1.817874
C	2.562403	-3.004244	-2.637397
H	4.595801	-1.896824	-4.312008
H	5.753546	0.291493	-3.240876
H	5.854026	2.261586	1.689198
H	4.623165	1.593020	3.992586
H	-0.093547	-0.529202	4.922190
H	-1.959053	-1.689248	3.351099
H	-1.533411	-4.556854	-1.120406
H	0.390430	-4.858888	-3.004570
C	-2.272420	-3.020494	0.981823
C	-3.132039	-2.583658	-0.040439
C	-2.846942	-3.630407	2.120176
C	-4.524121	-2.563504	0.141301
H	-2.712613	-2.134717	-0.943933
C	-4.241866	-3.696084	2.263993
H	-2.194568	-4.023343	2.903573
C	-5.088488	-3.108655	1.307509
H	-4.670057	-4.172436	3.149443
H	-6.169517	-3.074883	1.466022
C	-5.214909	-1.671542	-0.853572
O	-5.110791	-1.830556	-2.083235
N	-5.755217	-0.541246	-0.282832
H	-5.698381	-0.478299	0.733646
C	-5.763911	0.718809	-1.021669
H	-5.665400	0.447017	-2.083222

H	-6.728210	1.239700	-0.895116
Co	2.262533	-1.280735	0.321409
C	5.906916	1.812548	-0.972826
H	5.875559	2.012896	-2.051580
H	5.750784	2.772877	-0.461018
H	6.923507	1.464540	-0.725123
C	2.495985	0.276592	5.019800
H	1.961502	-0.418162	5.681888
H	3.541259	0.309964	5.356635
H	2.066044	1.281956	5.167805
C	2.789653	-3.827517	-3.889811
H	2.264587	-4.790266	-3.852590
H	2.447501	-3.290051	-4.790311
H	3.859733	-4.044193	-4.026073
C	-4.629692	1.699946	-0.592483
H	-4.852956	2.095385	0.412333
H	-4.711782	2.553824	-1.290295
C	-2.825153	0.590904	0.694867
C	-2.819537	0.569353	-1.829429
C	-2.439283	1.628475	1.756904
H	-1.952337	-0.055042	0.520184
H	-3.594967	-0.077502	1.127715
H	-3.014653	1.292195	-2.643803
H	-3.402402	-0.340472	-2.085746
C	-1.346985	0.173392	-1.867417
H	-3.256756	2.352137	1.911573
H	-2.244725	1.106374	2.714863
H	-1.115387	-0.633330	-1.139567
H	-1.107890	-0.230945	-2.870300
C	-0.056445	1.722434	1.625418
H	-0.032549	0.762787	1.080457
H	0.046702	1.486642	2.703118
C	0.841008	0.936991	-1.404659
H	0.919800	0.219812	-0.548619
H	1.247671	0.405274	-2.287910
C	1.105336	2.618982	1.215790
H	1.075039	3.541715	1.816734
H	2.056863	2.093313	1.413532
C	1.652587	2.197152	-1.125515
H	2.673476	1.911042	-0.815708
H	1.717699	2.803131	-2.042888
O	-0.524181	1.311505	-1.576110
O	1.040084	3.061991	-0.154910
O	-1.290134	2.414924	1.382975
N	-3.235220	1.225290	-0.573932
Ba	-1.553887	4.175761	-0.975953

## XV. Electrocatalytic CO<sub>2</sub> Reduction and Catalyst Deactivation

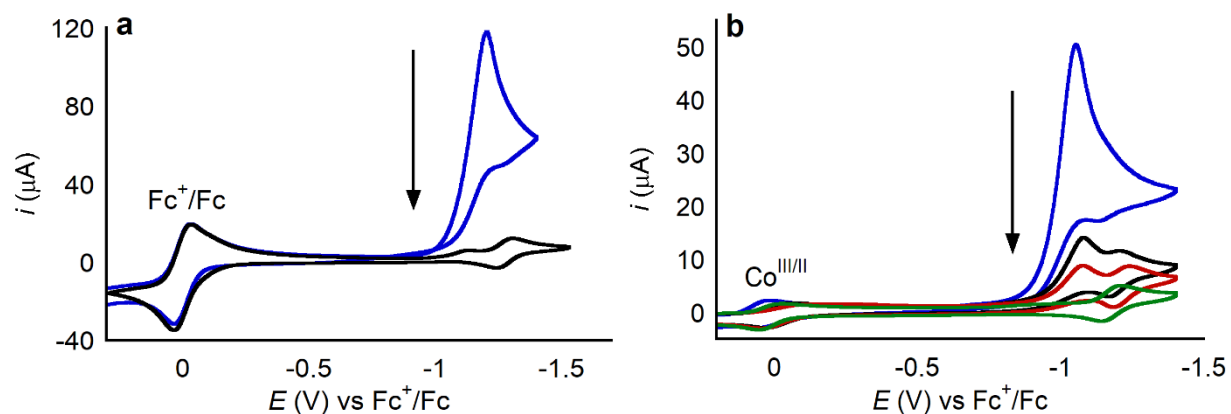


**Figure S51.** Representative cyclic voltammograms showing the deactivation of **1** under  $\text{CO}_2$  in the presence of (a) 10 mM TFE, and (b) no added proton source. The arrows indicate the decrease in current as consecutive voltammograms are collected. Cyclic voltammograms were collected at 100 mV/s in 0.25 M  $\text{TBAPF}_6$  MeCN containing 0.5 mM of **1**.

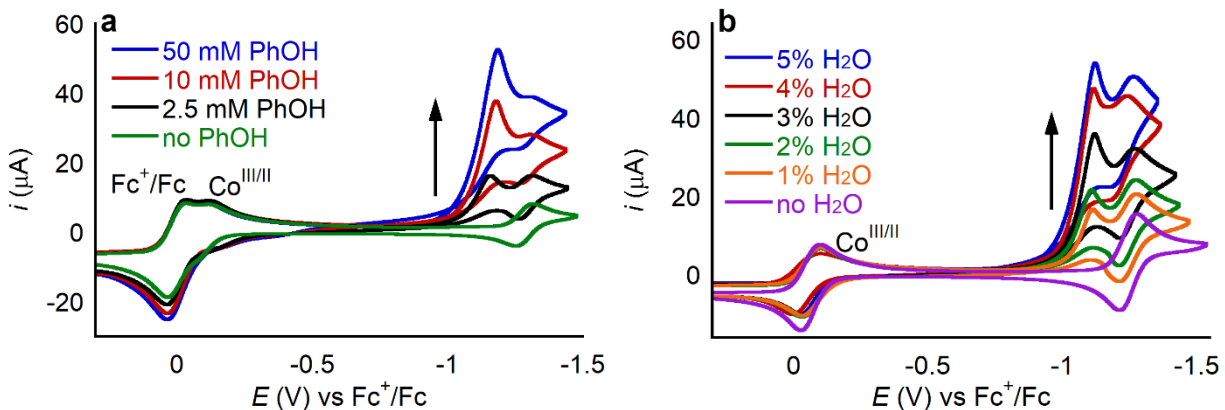


**Figure S52.** Cyclic voltammograms collected for **2** (0.5 mM) under  $\text{CO}_2$  upon addition of (a) phenol or (b) water, consistent with  $\text{CO}_2$  reduction occurring slightly anodic of the  $\text{Co(II)/Co(I)}$  couple. The arrows indicate the increase in current as the concentration of the proton source is increased. Voltammograms were collected at 100 mV/s in 0.25 M  $\text{TBAPF}_6$  in MeCN.

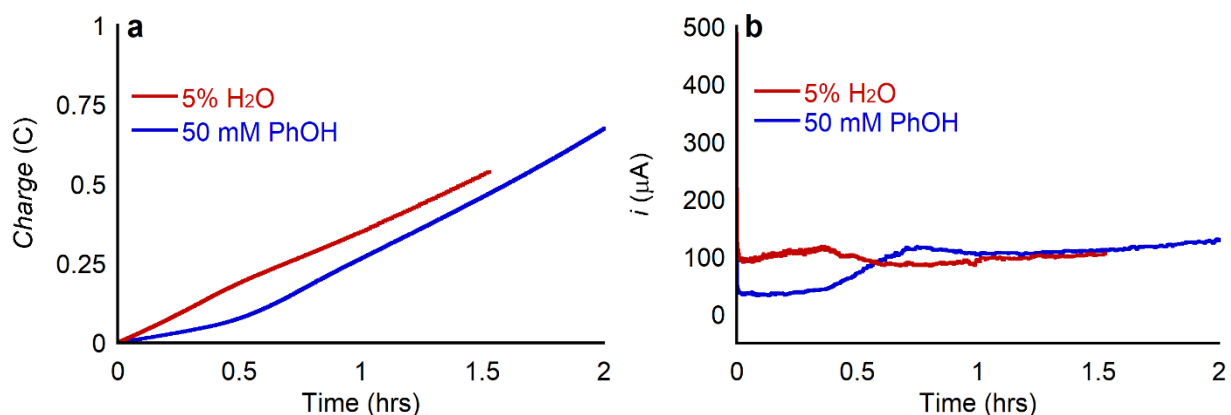


**Figure S53.** Controlled potential electrolysis for **2** (0.5 mM) at  $-1.15$  V vs  $\text{Fc}^+/\text{Fc}$  under  $\text{CO}_2$  with added proton source as indicated in the figures. Faradaic efficiencies for  $\text{CO}$  were 100 and 84% for water and phenol, respectively. No  $\text{H}_2$  was detected in either case. (a) Charge vs time trace and (b) current vs time trace.

## XVI. References

1. Stoll, S.; Schweiger, A. EasySpin, A Comprehensive Software Package for Spectral Simulation and Analysis in EPR. *J. Magn. Reson.* **2006**, *178*, 42.
2. Virtanen, P.; Gommers, R.; Oliphant, T. E.; Haberland, M.; Reddy, T.; Cournapeau, D.; Burovski, E.; Peterson, P.; Weckesser, W.; Bright, J.; van der Walt, S. J.; Brett, M.; Wilson, J.; Millman, K. J.; Mayorov, N.; Nelson, A. R. J.; Jones, E.; Kern, R.; Larson, E.; Carey, C. J.; Polat, İ.; Feng, Y.; Moore, E. W.; VanderPlas, J.; Laxalde, D.; Perktold, J.; Cimrman, R.; Henriksen, I.; Quintero, E. A.; Harris, C. R.; Archibald, A. M.; Ribeiro, A. H.; Pedregosa, F.; van Mulbregt, P.; Vijaykumar, A.; Bardelli, A. P.; Rothberg, A.; Hilboll, A.; Kloeckner, A.; Scopatz, A.; Lee, A.; Rokem, A.; Woods, C. N.; Fulton, C.; Masson, C.; Häggström, C.; Fitzgerald, C.; Nicholson, D. A.; Hagen, D. R.; Pasechnik, D. V.; Olivetti, E.; Martin, E.; Wieser, E.; Silva, F.; Lenders, F.; Wilhelm, F.; Young, G.; Price, G. A.; Ingold, G.-L.; Allen, G. E.; Lee, G. R.; Audren, H.; Probst, I.; Dietrich, J. P.; Silterra, J.; Webber, J. T.; Slavič, J.; Nothman, J.; Buchner, J.; Kulick, J.; Schönberger, J. L.; de Miranda Cardoso, J. V.; Reimer, J.; Harrington, J.; Rodríguez, J. L. C.; Nunez-Iglesias, J.; Kuczynski, J.; Tritz, K.; Thoma, M.; Newville, M.; Kümmerer, M.; Bolingbroke, M.; Tartre, M.; Pak, M.; Smith, N. J.; Nowaczyk, N.; Shebanov, N.; Pavlyk, O.; Brodtkorb, P. A.; Lee, P.; McGibbon, R. T.; Feldbauer, R.; Lewis, S.; Tygier, S.; Sievert, S.; Vigna, S.; Peterson, S.; More, S.; Pudlik, T.; Oshima, T. SciPy 1.0: Fundamental Algorithms for Scientific Computing in Python. *Nature Meth.* **2020**, *17*, 261.
3. Pracht, P.; Bohle, F.; Grimme, S. Automated Exploration of the Low-Energy Chemical Space with Fast Quantum Chemical Methods. *Phys. Chem. Chem. Phys.* **2020**, *22*, 7169.
4. Bannwarth, C.; Ehlert, S.; Grimme, S. GFN2-xTB-An Accurate and Broadly Parametrized Self-Consistent Tight-Binding Quantum Chemical Method with Multipole Electrostatics and Density-Dependent Dispersion Contributions. *J. Chem. Theory Comput.* **2019**, *15*, 1652.
5. Grimme, S. Exploration of Chemical Compound, Conformer, and Reaction Space with Meta-Dynamics Simulations Based on Tight-Binding Quantum Chemical Calculations. *J. Chem. Theory Comput.* **2019**, *15*, 2847.
6. Gaussian 16, Revision C.01, Frisch, M. J.; Trucks, G. W.; Schlegel, H. B.; Scuseria, G. E.; Robb, M. A.; Cheeseman, J. R.; Scalmani, G.; Barone, V.; Petersson, G. A.; Nakatsuji, H.; Li, X.; Caricato, M.; Marenich, A. V.; Bloino, J.; Janesko, B. G.; Gomperts, R.; Mennucci, B.; Hratchian, H. P.; Ortiz, J. V.; Izmaylov, A. F.; Sonnenberg, J. L.; Williams-Young, D.; Ding, F.; Lipparini, F.; Egidi, F.; Goings, J.; Peng, B.; Petrone, A.; Henderson, T.; Ranasinghe, D.; Zakrzewski, V. G.; Gao, J.; Rega, N.; Zheng, G.; Liang, W.; Hada, M.; Ehara, M.; Toyota, K.; Fukuda, R.; Hasegawa, J.; Ishida, M.; Nakajima, T.; Honda, Y.; Kitao, O.; Nakai, H.; Vreven, T.; Throssell, K.; Montgomery, J. A., Jr.; Peralta, J. E.; Ogliaro, F.; Bearpark, M. J.; Heyd, J. J.; Brothers, E. N.; Kudin, K. N.; Staroverov, V. N.; Keith, T. A.; Kobayashi, R.; Normand, J.; Raghavachari, K.; Rendell, A. P.; Burant, J. C.; Iyengar, S. S.; Tomasi, J.; Cossi, M.; Millam, J. M.; Klene, M.; Adamo, C.; Cammi, R.; Ochterski, J. W.; Martin, R. L.; Morokuma, K.; Farkas, O.; Foresman, J. B.; Fox, D. J. Gaussian, Inc., Wallingford CT, 2016.
7. (a) Perdew, J. P. Density-Functional Approximation for the Correlation-Energy of the Inhomogeneous Electron-Gas. *Phys. Rev. B* **1986**, *33*, 8822; (b) Becke, A. D. Density-Functional Exchange-Energy Approximation with Correct Asymptotic-Behavior. *Phys. Rev. A* **1988**, *38*, 3098.
8. Grimme, S.; Antony, J.; Ehrlich, S.; Krieg, H. A Consistent and Accurate Ab Initio Parametrization of Density Functional Dispersion Correction (DFT-D) for the 94 Elements H-Pu. *J. Chem. Phys.* **2010**, *132*, 154104.
9. (a) Wadt, W. R.; Hay, P. J. Abinitio Effective Core Potentials for Molecular Calculations - Potentials for Main Group Elements Na to Bi. *J. Chem. Phys.* **1985**, *82*, 284; (b) Hay, P. J.; Wadt, W. R. Abinitio Effective Core Potentials for Molecular Calculations - Potentials for K to Au Including the Outermost Core Orbitals. *J. Chem. Phys.* **1985**, *82*, 299.
10. (a) Hehre, W. J.; Ditchfield, R.; Pople, J. A. Self-Consistent Molecular-Orbital Methods. XII. Further Extensions of Gaussian-Type Basis Sets for Use in Molecular-Orbital Studies of Organic-Molecules. *J. Chem. Phys.* **1972**, *56*, 2257; (b) Hariharan, P. C.; Pople, J. A. Influence of Polarization Functions on Molecular-Orbital Hydrogenation Energies. *Theor. Chim. Acta.* **1973**, *28*, 213.

11. Barone, V.; Cossi, M. Quantum Calculation of Molecular Energies and Energy Gradients in Solution by a Conductor Solvent Model. *J. Phys. Chem. A* **1998**, *102*, 1995.
12. Zhang, X. L., F.; Cao, M.; Zhong, M. Rare Earth–Cobalt Bimetallic Catalysis Mediates Stereocontrolled Living Radical Polymerization of Acrylamides. *Nature Synth.* **2023**, *2*, 855.